Astronomy & Astrophysics manuscript no. AA˙2008˙11519
June 29, 2009

High-energy emission from jet-clump interactions in microquasars

A. T. Araudo[1,2,⋆], V. Bosch-Ramon[3] and G. E. Romero[1,2,⋆⋆]

[1] Instituto Argentino de Radioastronomía (CCT La Plata, CONICET), C.C.5, 1894 Villa Elisa, Buenos Aires, Argentina
[2] Facultad de Ciencias Astronómicas y Geofísicas, Universidad Nacional de La Plata, Paseo del Bosque, 1900 La Plata, Argentina
[3] Max Planck Institut für Kernphysik, Saupfercheckweg 1, Heidelberg 69117, Germany

Received / Accepted

ABSTRACT

Context. High-mass microquasars are binary systems consisting of a massive star and an accreting compact object from which relativistic jets are launched. There is considerable observational evidence that winds of massive stars are clumpy. Individual clumps may interact with the jets in high-mass microquasars to produce outbursts of high-energy emission. Gamma-ray flares have been detected in some high-mass X-ray binaries, such as Cygnus X-1, and probably in LS 5039 and LS I+61 303.
Aims. We predict the high-energy emission produced by the interaction between a jet and a clump of the stellar wind in a high-mass microquasar.
Methods. Assuming a hydrodynamic scenario for the jet-clump interaction, we calculate the spectral energy distributions produced by the dominant non-thermal processes: relativistic bremsstrahlung, synchrotron and inverse Compton radiation, for leptons, and for hadrons, proton-proton collisions.
Results. Significant levels of emission in X-rays (synchrotron), high-energy gamma rays (inverse Compton), and very high-energy gamma rays (from the decay of neutral pions) are predicted, with luminosities in the different domains in the range $\sim 10^{32}$-10^{35} erg s^{-1}. The spectral energy distributions vary strongly depending on the specific conditions.
Conclusions. Jet-clump interactions may be detectable at high and very high energies, and provide an explanation for the fast TeV variability found in some high-mass X-ray binary systems. Our model can help to infer information about the properties of jets and clumpy winds by means of high-sensitivity gamma-ray astronomy.

Key words. Gamma-rays: theory – X-rays: binaries – Radiation mechanisms: non-thermal

1. Introduction

The mass loss in massive and hot stars is understood to occur by means of supersonic inhomogeneous winds structured as very dense and small clumps embedded in large regions of tenuous plasma. This idea is supported by considerable observational evidence of the clumpy structure of these winds (e.g. Puls et al. 2006, Owocki & Cohen 2006, Moffat 2008). However, as a consequence of the high spatial resolution necessary for a straightforward detection of the clumps, all the evidence is indirect. Hence, properties of clumps, such as size, density, and number, are not well-known.

Some massive stars are accompanied by a compact object, to which they transfer matter. This process leads to the formation of an accretion disk around the compact object and, in high-mass microquasars (HMMQs), to the generation of bipolar relativistic outflows (e.g. Mirabel & Rodríguez 1999).

Non-thermal emission has been observed in microquasar jets from radio (e.g. Ribó 2005) to X-rays (e.g. Corbel et al. 2002). At higher energies, gamma-ray radiation could also be produced in jets (e.g. Bosch-Ramon et al. 2006). A TeV flare was detected by MAGIC from the HMMQ Cygnus X-1 (Albert et al. 2007). Transient gamma-ray events may also have been detected from the high-mass X-ray binaries LS 5039 and LS I+61 303 by HESS (Aharonian et al. 2005) and MAGIC (Albert et al. 2006), respectively, as suggested by Paredes (2008). In addition, the HMMQ Cygnus X-3 might have been observed flaring in the GeV range by *AGILE* (ATels 1492, 1547 and 1585, see however Atel 1850). Both this instrument and *Fermi* also found several transient GeV sources in the Galactic plane without known counterpart (ATel 1394, Abdo et al. 2009). All this strongly variable gamma-ray emission may have a similar origin. For instance, the interaction between the jet and the stellar wind of the companion star could produce TeV flares (e.g., Romero et al. 2003, Romero & Orellana 2005, Romero et al. 2007, Albert et al. 2007, Perucho & Bosch-Ramon 2008, Owocki et al. 2009).

In this paper, we propose a model to explain these gamma-ray flares, based on the interaction between the jets of a HMMQ with wind inhomogeneities. The clumps can eventually penetrate the jet, leading to transient non-thermal activity that may release a significant fraction of the jet kinetic luminosity in the form of synchrotron, inverse Compton (IC), and proton-proton (pp) π^0-decay emission.

This work is organized as follows. In the next section, we describe the main characteristics of the scenario adopted and estimate the relevant timescales of the jet-clump inter-

Send offprint requests to: Anabella T. Araudo: *aaraudo@fcaglp.unlp.edu.ar*
⋆ Fellow of CONICET, Argentina
⋆⋆ Member of CONICET, Argentina

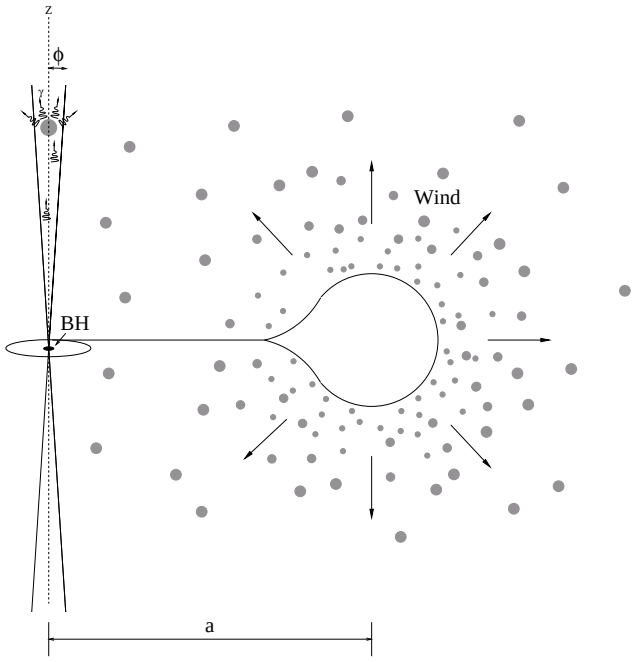

Fig. 1. Sketch of a HMMQ with clumpy stellar wind, adapted from Romero et al. (2007).

action; in Sect. 3, we study the acceleration of particles and estimate the non-thermal radiative losses; in Sect. 4, we describe the calculation of the non-thermal emission and present the main results; and finally, in Sect. 5, we draw some conclusions. CGS units are used consistently throughout the paper.

2. The physical scenario

To study the interaction between a clump of the stellar wind and a jet in a HMMQ, we adopt a scenario with similar characteristics to the binary system Cygnus X-1. We fix the separation between the compact object and the massive star to be $a = 3\times10^{12}$ cm (0.2 UA). For the star luminosity and temperature, we assume that $L_\star = 10^{39}$ erg s^{-1} and $T_\star = 3\times10^4$ K, and the stellar mass loss rate is adopted to be $\dot{M}_\star = 3\times10^{-6}\,M_\odot$ yr^{-1}, with a terminal wind velocity $v_\mathrm{w} \sim 2.5\times10^8$ cm s^{-1}. A sketch of the scenario is presented in Fig. 1.

2.1. Clump model

The clump is assumed to be spherical and homogeneous. Given the uncertainties in the clump parameters, we consider two values of its size: $R_\mathrm{c} = 10^{10}$ and 10^{11} cm (i.e., $\sim 3\times(10^{-3}-10^{-2})\,a$). For effective jet penetration, a large density contrast between the clump and the jet is required. Therefore, we assume dense clumps with $n_\mathrm{c} = 10^{12}$ cm^{-3}, which correspond to a porous clumpy wind with a filling factor (clump versus interclump volume ratio) of $f = \dot{M}_\star/4\pi a^2 m_p v_\mathrm{c} n_\mathrm{c} = 0.005$, where m_p is the mass of the proton[1]. We assume that the velocity of the clumps equals the velocity of the wind, i.e., $v_\mathrm{c} = 2.5\times10^8$ cm s^{-1}. The temperature of the clumps is taken as $T_\mathrm{c} = 10^4$ K (Krtička & Kubát 2001), which is moderately lower than the temperature at the surface of the massive star.

[1] See Owocki & Cohen (2006) for the concept of a porous wind.

Table 1. Adopted parameters in this work.

Parameter description [units]	Clump	Jet
Radius [cm]	$10^{10}-10^{11}$	1.5×10^{11}
Velocity [cm s^{-1}]	2.5×10^8	10^{10}
Density [cm^{-3}]	10^{12}	4.7×10^7
	Binary system	
System size [cm]	3×10^{12}	
Star luminosity [erg s^{-1}]	10^{39}	
Star temperature [K]	3×10^4	
Mass loss rate [M$_\odot$ yr^{-1}]	3×10^{-6}	
Wind velocity [cm s^{-1}]	2.5×10^8	

2.2. Jet model

Radio observations demonstrated that the jets of MQs are strongly collimated (Miller-Jones, Fender & Nakar 2006). We assume that the jet radius is one tenth of the jet height, i.e. $R_\mathrm{j}(z) = 0.1\,z$, which corresponds to a semi-opening angle of $\phi = 6°$. The expansion velocity results in $v_\mathrm{exp} = 0.1\ v_\mathrm{j}$, where v_j is the velocity of the jet. This expansion velocity for a free-expanding hidrodynamical jet implies a jet base Mach number $\sim v_\mathrm{j}/v_\mathrm{exp} \sim 10$, i.e. a strongly supersonic outflow. We consider a jet dynamically dominated by cold protons with a weakly relativistic bulk velocity $v_\mathrm{j} = 0.3\,c$, i.e. a Lorentz factor $\gamma_\mathrm{j} = 1.06$. We neglect the curvature of the jet produced by its interaction with the stellar wind. In HMMQ jets of luminosity $> 10^{36}$ erg s^{-1}, the geometry should not be strongly modified (Perucho & Bosch-Ramon 2008), although this effect could be important in systems such as Herbig-Haro jets interacting with a stellar wind, as studied by Raga et al. (2009).

The kinetic luminosity of the jet is taken to be $L_\mathrm{kin} \sim 3\times10^{36}$ erg s^{-1}, similar to that of Cygnus X-1 (e.g., Gallo et al. 2005, Russell et al. 2007). Using the equation

$$L_\mathrm{kin} = \sigma_\mathrm{j}(\gamma_\mathrm{j}-1)m_p\,c^2\,n_\mathrm{j}\,v_\mathrm{j}, \quad (1)$$

where $\sigma_\mathrm{j} = \pi R_\mathrm{j}^2$ is the cross-section of the jet, we can estimate the density n_j of the jet material in the laboratory reference frame (LRF). At the height of the jet-clump interaction, which is taken to occur at $z = a/2$, we obtain $n_\mathrm{j} = 4.7\times10^7$ cm^{-3}. Thus, the ratio of the clump to the jet densities is $\chi = 2.1\times10^4$. This parameter will be very relevant to the jet-clump interaction estimates. The parameter values of the clump and the jet are shown in Table 1. We assume an ideal gas equation of state, $P = nkT$, for both the clump and the jet, where n is the gas density.

2.3. Dynamics of the interaction

Clumps are formed in the wind acceleration region within one stellar radius of the surface of the star (e.g. Puls et al. 2006) and some of them reach the jet/wind interface. The very large inertia of the clumps, linked to the exceptionally high density contrast χ, allows them to cross the boundary of the jet and fully penetrate into it. A large value of χ is also required to ensure that the clump is not strongly affected when penetrating into the jet.

To study the physical processes of the interaction, we consider the collision of a single clump with the jet. For simplicity, we assume that, on the relevant spatial scales of the interaction, the jet is cylindrical. In the context of this work, thermal conduction, clump expansion, magnetic fields and gravitational forces are not dynamically relevant and will be neglected.

In the LRF, the clump will take a time $t_{\rm c}$, or jet penetration time, to fully enter the jet. This provides the first relevant timescale

$$t_{\rm c} \sim 2\,R_{\rm c}/v_{\rm c}, \tag{2}$$

which is $t_{\rm c} \sim 80$ and ~ 800 s, for $R_{\rm c} = 10^{10}$ and 10^{11} cm, respectively. In addition, the clump crosses the jet roughly at the wind velocity in the jet-crossing time

$$t_{\rm j} \sim \frac{2\,R_{\rm j}}{v_{\rm c}} = 1.2\times10^{3}\ {\rm s}. \tag{3}$$

From the moment when the clump interacts with the jet, the ram pressure exerted by the latter produces a shock in the clump, which propagates in the direction of the jet motion. Assuming that a significant fraction of the momentum flux is transferred to the clump, the clump-crossing time, which is the characteristic timescale of the jet-clump interaction, can be defined to be

$$t_{\rm cc} \sim \frac{2\,R_{\rm c}}{v_{\rm cs}} \sim \frac{2\,R_{\rm c}\sqrt{\chi}}{v_{\rm j}}, \tag{4}$$

where

$$v_{\rm cs} \sim \frac{v_{\rm j}}{\sqrt{\chi}} \tag{5}$$

is the velocity of the shock moving through the clump, derived by equating the jet/clump ram pressures. The timescale $t_{\rm cc}$ is $\sim 3\times10^{2}$ and 3×10^{3} s for $R_{\rm c} = 10^{10}$ and 10^{11} cm, respectively.

A shock (the bow shock) is also formed in the jet when its material collides with the clump. We assume that the bow-shock region width (or clump/bow-shock separation distance) is $x \sim 0.2R_{\rm c}$ (van Dyke & Gordon 1959), and thus the time required to reach the steady state regime is

$$t_{\rm bs} \sim \frac{0.2R_{\rm c}}{v_{\rm j\ ps}}, \tag{6}$$

where $v_{\rm j\ ps} \sim v_{\rm j}/4$ is the jet postshock velocity in the LRF. Therefore, $t_{\rm bs} \sim (5/2)t_{\rm cc}/\sqrt{\chi}$, i.e. $t_{\rm bs} \ll t_{\rm cc}$. In Fig. 2, a sketch of the situation is shown.

Once the clump is inside the jet, the latter transfers momentum to the clump, accelerating it to the background velocity, $v_{\rm j}$. The acceleration can be obtained from the force exerted by the jet ram pressure and the clump mass (e.g., Fragile et al. 2004):

$$g \sim \frac{v_{\rm j}^2}{\chi R_{\rm c}}\,. \tag{7}$$

The jet accelerates the clump to the velocity $v_{\rm j}$ in a time

$$t_{\rm g} \sim \frac{v_{\rm j}}{g} \sim \sqrt{\chi}\,t_{\rm cc}, \tag{8}$$

which is much longer than $t_{\rm cc}$. When one fluid exerts a force against another fluid of different density, the hydrodynamical Rayleigh-Taylor (RT) instability eventually develops,

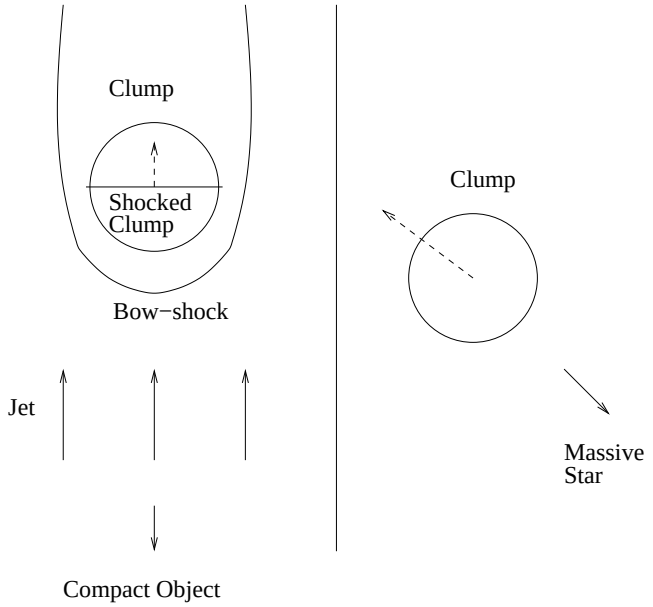

Fig. 2. Sketch of the jet-clump interaction.

leading to the perturbation and potential disruption of the clump. The timescale for this instability is

$$t_{\rm RT} \sim \sqrt{l/g}, \tag{9}$$

where l is the instability length in the perturbed region.

After the bow shock is formed, the jet material surrounds the clump and we have two fluids that have a large relative velocity. This situation leads to Kelvin-Helmholtz (KH) instabilities. The timescale for a KH instability to develop is

$$t_{\rm KH} \sim \frac{l\,\sqrt{\chi}}{v_{\rm rel}}, \tag{10}$$

where $v_{\rm rel}$ is the relative velocity between the jet material and the clump material (we assume $v_{\rm rel} \sim v_{\rm j}$). In addition, taking into account that we are interested in instability lengths similar to the clump size, i.e. $l \sim R_{\rm c}$, we find that $t_{\rm RT} \sim t_{\rm KH} \sim t_{\rm cc}$.

According to the timescales estimated in the previous paragraphs, the clump can fully enter into the jet if $t_{\rm c} \approx t_{\rm cc}/5$. At this stage, we do not consider the penetration of the clump into the jet, and assume that the former is completely inside the latter (i.e., the system has cylindrical symmetry). The bow shock is formed in a time much shorter than $t_{\rm c}$ and $t_{\rm cc}$ ($t_{\rm bs} \sim t_{\rm cc}/\sqrt{\chi}$). We note that the clump might not escape the jet if $t_{\rm j} > t_{\rm RT/KH}$. In such a case, the clump will be destroyed inside the jet. However, numerical simulations show that the instability timescales are longer than the clump crossing time by a factor of a few (e.g., Klein, McKee & Colella 1994), i.e., $t_{\rm RT/KH} > t_{\rm cc}$.

Regarding the shock properties and given the particular characteristics of our scenario, the shock in the clump is strong, radiative, and slow, whereas the bow shock is strong as well, but adiabatic and fast. For these reasons, the shocked and heated material of the clump will radiate a non-negligible part of the energy tranferred by the jet.

2.3.1. Thermal emission from the clump

To estimate the density, $n_{\rm ps}(\zeta)$, and temperature, $T_{\rm ps}(\zeta)$, of the shocked clump at a distance ζ from the shock, we assume pressure equilibrium between the clump and the jet shocked plasma and use the equation of energy flux conservation, taking into account the main channels of thermal radiative losses: $\Lambda(T) = 7\times10^{-19}\,T^{-0.6}$ erg cm^{-3} s^{-1}. The timescale of thermal cooling equals

$$t_{\rm th} = 3\times10^2\frac{T_{\rm ps}(\zeta)^{1.6}}{n_{\rm ps}(\zeta)}\,{\rm s}\,. \quad (11)$$

The temperature and density in the adiabatic zone of the post-shock region are 8.5×10^6 K and 4×10^{12} cm^{-3}, respectively. From these values, the shocked clump material cools in a time $t_{\rm th}\sim10$ s, which is shorter than $t_{\rm cc}$, which means a distance $\zeta_{\rm th}\sim t_{\rm th}\,v_{\rm cs}/4\sim2\times10^8$ cm from the shock front. Since $\zeta_{\rm th}<2R_{\rm c}$, the shock in the clump is radiative. At distances greater than $\zeta_{\rm th}$, the density of the shocked matter can reach values as high as 10^{14} cm^{-3}.

Although we are mainly interested in the high-energy emission produced by the jet-clump interaction, we estimate for comparison the free-free emission generated by the shocked and heated clump. Considering $T_{\rm ps}(\zeta)$ and $n_{\rm ps}(\zeta)$, we estimate the free-free luminosity by integrating the emissivity (Lang 1999) along the shocked clump, as demonstrated in Zhekov & Palla (2007). The corresponding thermal luminosities are $L_{\rm th}\sim5\times10^{30}$ and 5×10^{32} erg s^{-1} for $R_{\rm c}=10^{10}$ and 10^{11} cm, respectively, peaking in the soft X-rays. In Fig. 7, the thermal radiation of the clump is shown together with the non-thermal emission.

In contrast to what occurs in the clump, the bow shock is adiabatic and fast. For this reason, it is a propitious place to accelerate particles to relativistic energies.

3. Particle acceleration and non-thermal cooling

3.1. Particle acceleration

In the presence of a shock and magnetic field, non-relativistic diffusive (Fermi I) shock acceleration can occur (e.g. Drury 1983). In the linear limit of this theory and considering Bohm diffusion, electrons and protons will be accelerated to an energy $E_{e,p}$ (where e stands for electrons and p for protons) in a time

$$t_{\rm acc} = \eta\frac{E_{e,p}}{q\,B\,c}\,, \quad (12)$$

where $\eta\sim(8/3)(c/v_{\rm s})^2$ for perpendicular shocks (Protheroe 1999). In Eq. (12), $v_{\rm s}$ is the shock velocity (taken to be equal to $v_{\rm j}$), B is the magnetic field in the acceleration region, c is the speed of light, and q is the electron charge. Thus, to obtain efficient acceleration of particles, i.e., a short $t_{\rm acc}$, a high value of B and a strong and fast shock are necessary.

To study the jet-clump interaction, we consider two values of the magnetic field in the jet shocked (bow-shock) region, $B_{\rm bs}$. First, we consider a value of the magnetic field obtained by assuming that the magnetic energy density is 10 % of the plasma internal energy density downstream. We adopt a sub-equipartition value to ensure that $B_{\rm bs}$ is dynamically negligible with respect to matter. Fixing

$$\frac{B_{\rm bs}^2}{8\pi} = 0.1u_p\,, \quad (13)$$

where u_p is the energy density of the shocked jet gas, given by

$$u_p = \frac{3}{2}P = \frac{9}{8}\,n_{\rm j}\,m_p v_{\rm j}^2\,, \quad (14)$$

we obtain $B_{\rm bs}=150$ G. This magnetic field, plus $v_{\rm s}=v_{\rm j}$, yield $t_{\rm acc}\sim10^{-2}E_{e,p}$ s.

In addition, we adopt $B_{\rm bs}=1$ G to check the impact on our results of a magnetic field significantly weaker than in the sub-equipartition case.

3.2. Non-thermal cooling processes

Relativistic leptons lose their energy by different non-thermal radiative processes, such as synchrotron radiation, IC scattering and relativistic bremsstrahlung. On the other hand, relativistic protons can also lose energy by means of *pp* interactions. Finally, the shocked plasma can produce thermal radiation if the density is high enough, as shown in Sect. 2.3.1.

Relativistic electrons that lose their energy by synchrotron radiation have the following cooling time (e.g. Ginzburg & Syrovatskii, 1964)

$$t_{\rm syn} = \frac{4.1\times10^2}{B^2\,E_e}\,{\rm s}\,. \quad (15)$$

Synchrotron radiation is the most efficient radiative process in the bow-shock region in the case of $B_{\rm bs}=150$ G, where $t_{\rm synch}\sim2\times10^{-2}\,E_e^{-1}$ s.

At the interaction height considered in this work, $z_{\rm int}=a/2=1.5\times10^{12}$ cm, the energy density of the photons from the star is $u_{\rm ph}=2.4\times10^2$ erg cm^{-3}, the typical photon energy being $\epsilon_0\sim10$ eV. For $y=\epsilon_0E_e/(5.1\times10^5\,{\rm eV})^2>1$, i.e. $E_e>2.6\times10^{10}$ eV, the IC interaction occurs in the Klein-Nishina (KN) regime. A formula for the IC cooling time valid in both a Thompson (Th) and KN regime in a photon field with a narrow energy distribution is e.g. Bosch-Ramon & Khangulyan (2009)

$$t_{\rm IC} = \frac{6.1\times10^{12}\,\epsilon_0}{u_{\rm ph}}\frac{(1+8.3y)}{\ln(1+0.2\,y)}\frac{(1+1.3y^2)}{(1+0.5y+1.3y^2)}\,{\rm s}\,. \quad (16)$$

For $B\sim1$ G, IC is the dominant loss leptonic channel.

According to the low particle density of the shocked jet, $n_{\rm bs}=4\,n_{\rm j}=2\times10^8$ cm^{-3}, relativistic bremsstrahlung losses are negligible in the bow-shock region, the cooling time for a completely ionized medium being (e.g. Blumenthal & Gould, 1970):

$$t_{\rm Brem} = \frac{1.4\times10^{16}}{n\,Z^2\left(\ln\left(\frac{E_e}{m_ec^2}\right)+0.36\right)}\,{\rm s}\,, \quad (17)$$

where Z is the atomic number, and in our case $Z=1$.

Regarding hadronic emission, γ-rays are produced if relativistic protons interact with nuclei through inelastic collisions. As in the case of relativistic bremsstrahlung, the proton cooling time due to *pp* interactions depends on the density n (e.g. Aharonian & Atoyan, 1996) related

$$t_{pp}\sim\frac{2\times10^{15}}{n}\,{\rm s}\,. \quad (18)$$

In the bow-shock region, this process is negligible. Otherwise, if relativistic protons accelerated in the bow shock penetrate into the clump, *pp* interactions can become an efficient process to generate gamma-rays.

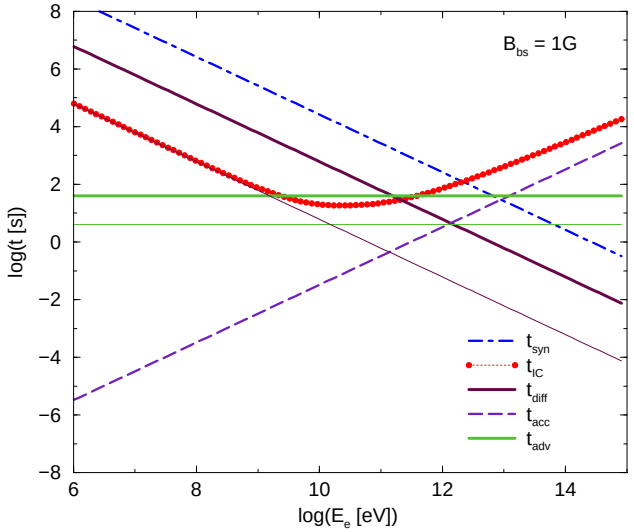

Fig. 3. Acceleration and radiative loss (synchrotron and IC) time for electrons in the bow-shock region. The advection and diffusion times are shown for $R_{\rm c} = 10^{10}$ (thin line) and 10^{11} cm (thick line). This figure corresponds to the case $B_{\rm bs} = 1$ G.

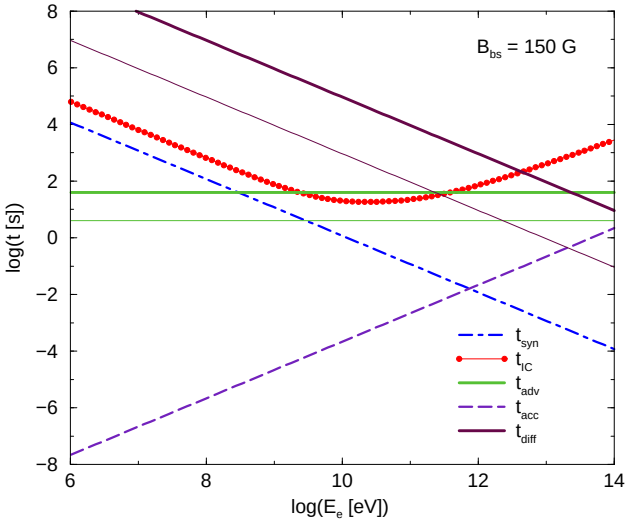

Fig. 4. Acceleration and radiative loss (synchrotron and IC) time for electrons in the bow-shock region. The advection and diffusion times are shown for $R_{\rm c} = 10^{10}$ (thin line) and 10^{11} cm (thick line). This figure corresponds to the case $B_{\rm bs} = 150$ G.

3.3. Maximum energies

Taking into account energy gains and losses, the maximum energy achieved by particles accelerated in the bow shock can be easily estimated. Concerning energy losses, we consider radiative cooling (described above) and the escape of particles. The latter takes into account the advection of relativistic particles by downstream bow-shock material ($t_{\rm adv} \sim R_{\rm c}/v_{\rm j\,ps}$) and the diffusion of particles ($t_{\rm diff} \sim x^2/2D_{\rm B}$, where $x = 0.2\,R_{\rm c}$ and $D_{\rm B} = E_{e,p}c/3qB_{\rm bs}$ is the diffusion coefficient, which is assumed to be the Böhm one). The corresponding timescale is

$$\tau_{\rm esc} = \min\{{\rm t}_{\rm diff}, {\rm t}_{\rm adv}\}\,. \quad (19)$$

Given the small thickness of the bow-shock region, we assume that particles that escape via diffusion go to the clump.

For electrons, the maximum energy is constrained by the escape of particles via diffusion ($B_{\rm bs} = 1$ G) and by synchrotron radiation ($B_{\rm bs} = 150$ G), as it is shown in Figs. 3 and 4. From these figures, we determine that the most relevant radiative process in the bow-shock region can be IC scattering if $B_{\rm bs} = 1$ G, and synchrotron radiation if $B_{\rm bs} = 150$ G. On the other hand, the maximum energy for protons accelerated in the bow shock is constrained by the Hillas criterion (Hillas 1984), i.e. when the proton gyroradius becomes equal to the size of the acceleration region:

$$E_p^{\rm max} = x\,q\,B_{\rm bs} = 0.2\,R_{\rm c}\,q\,B_{\rm bs}\,. \quad (20)$$

In Table 2, maximum energies for electrons and protons of different values of $B_{\rm bs}$ and $R_{\rm c}$ are shown.

4. Production of gamma-rays and lower energy radiation

We calculated the spectral energy distribution (SED) of the emission produced by the most relevant non-thermal radiative processes. In the bow-shock region, we considered synchrotron and IC radiation, and in the clump, we also considered relativistic bremsstrahlung and *pp*.

Table 2. Maximum energies achieved by acelerated particles in the bow shock. The values are in eV units and represent the different values of $R_{\rm c}$ and B studied in this work.

$R_{\rm c}$ [cm]	10^{10}	10^{10}	10^{11}	10^{11}
$B_{\rm bs}$ [G]	1	150	1	150
$E_e^{\rm max}$ [eV]	1.5×10^{11}	8×10^{11}	1.5×10^{12}	8×10^{11}
$E_p^{\rm max}$ [eV]	6×10^{11}	9×10^{13}	6×10^{12}	9×10^{14}

4.1. Distribution of relativistic particles

We assume an injected population of relativistic particles (electrons and protons) in the bow-shock region that follows a power-law energy distribution of the form

$$Q_{e,p}(E_{e,p}) = K_{e,p}\,E_{e,p}^{-\Gamma}\,\exp(-E_{e,p}/E_{e,p}^{\rm max})\,. \quad (21)$$

The index Γ is fixed to 2, typical of linear diffusive shock acceleration, and we add an exponential cut-off at high energies. The normalization constant $K_{e,p}$ is determined by assuming that 25 % of the jet luminosity incident on the bow shock, i.e. $\sim(\sigma_{\rm c}/\sigma_{\rm j})L_{\rm kin}$ (where $\sigma_{\rm c} = \pi R_{\rm c}^2$ is the clump effective cross section [2]), is converted into power of the accelerated particles. We note that the predicted fluxes scale linearly with the adopted non-thermal fraction.

To estimate the particle energy distribution $N_{e,p}$, we solve the kinetic equation in the one-zone model approxima-

[2] We neglect here the region where the bow shock becomes strongly oblicuous, and focus on where this shock is the strongest, i.e. right in front of the clump.

tion for the bow-shock region (e.g. Ginzburg & Syrovatskii 1964)

$$\frac{\partial N_{e,p}}{\partial t} = \frac{\partial}{\partial E_{e,p}}(P_{e,p}N_{e,p}) - \frac{N_{e,p}}{\tau_{\rm esc}} + Q_{e,p}\,, \quad (22)$$

where t is the time and $P_{e,p} = -\partial E_{e,p}/\partial t$ is the energy loss rate for particles.

The relativistic leptons reach the steady state well before the shock has crossed the clump. As shown in Figs. 3 and 4, the most energetic electrons can diffuse to the clump ($B_{\rm bs} = 1$ G) or lose their energy inside the bow-shock region by synchrotron and IC radiation ($B_{\rm bs} = 150$ G). However, particles downstream with low energies escape advected in the shocked material of the jet before cooling radiatively, producing a break in the energy spectrum of particles. By equating the advection and synchrotron loss times, we can estimate the break energy in the case with $B_{\rm bs} = 150$ G, which results in $E_{\rm b} = 3\times10^9$ and $E_{\rm b} = 3\times10^8$ eV, for $R_{\rm c} = 10^{10}$ and 10^{11} cm, respectively. For the case of $B_{\rm bs} = 1$ G, the break energy is determined by the advection and diffusion times, given $E_{\rm b} = 0.3E_e^{\rm max}$. The electrons with energies $E_e > E_{\rm b}$ can reach the clump and radiate inside it. The energy distribution of these electrons is

$$N_e^{\rm c}(E_e) \sim Q_e^{\rm c}(E_e)\, t_{\rm cool}\,, \quad (23)$$

where $Q_e^{\rm c}$ is the part of Q_e that corresponds to $0.3\,E_e^{\rm max} < E_e < E_e^{\rm max}$, and $t_{\rm cool} = 1/(t_{\rm syn}^{-1} + t_{\rm IC}^{-1} + t_{\rm Brem}^{-1} + t_{\rm ion}^{-1})$. The ionization cooling term, $t_{\rm ion} \sim 2\times10^{18}\,(E_e/n)$ s, comes from the high densities in the clump.

As noted in Sect. 3.2, relativistic protons do not suffer significant pp losses in the bow-shock region ($t_{\rm diff} \ll t_{pp}$). These protons can also reach the clump if they are not advected by the shocked material of the jet. By assuming that $t_{\rm diff} < t_{\rm adv}$, the minimum energy necessary to reach the clump is

$$E_p^{\rm min} = 0.025E_p^{\rm max}\,, \quad (24)$$

and the maximum energies of these protons are determined by the Hillas criterion and shown in Table 2. On the other hand, to confine relativistic protons in the clump, the magnetic field must be $> 10^3$ G, much stronger than the expected clump magnetic field[3], i.e., the protons will cross the entire clump in a time $\sim R_{\rm c}/c < t_{pp}$. We note that $R_{\rm c}$ should be the shocked clump width if the clump has already been affected by the shock. The distribution of relativistic protons in the clump is

$$N_p(E_p) = \frac{R_{\rm c}}{c}\,Q_p(E_p)\,. \quad (25)$$

With the steady distributions of relativistic electrons in the bow shock, $N_e(E_e)$, and of both electrons and protons in the clump, $N_e^{\rm c}(E_e)$ and $N_p(E_p)$, respectively, we can calculate the SEDs of the radiation produced by these particles.

4.2. Non-thermal emission from the bow shock

Since the energy density of the synchrotron emission is lower than that of the magnetic and stellar fields, synchrotron self-Compton processes will be neglected in our calculations.

[3] Assuming equipartition, magnetic fields ~ 100 G would be expected.

Synchrotron radiation is computed using the standard formulae given in Blumenthal & Gould (1970). Assuming that the distribution of relativistic electrons in the bow-shock region is isotropic and moves with a non-relativistic advection speed, we calculate the synchrotron SED as

$$\epsilon L_{\rm synch}(\epsilon) = \epsilon \int_{E_e^{\rm min}}^{E_e^{\rm max}} N_e(E_e)\; P(E_e,\epsilon)\, dE_e\,, \quad (26)$$

where

$$P(E_e,\epsilon) = 10^{34} B_{\rm bs} (\epsilon/E_{\rm c})^{(1/3)} \exp(-\epsilon/E_{\rm c})\,{\rm s}^{-1} \quad (27)$$

is the power function. The magnitude $E_{\rm c}(E_e) = 5.1\times10^{-8}\,B\,E_e^2$ erg is the characteristic energy of the produced photons.

For a thermal distribution of target photons, we can estimate the IC emission from

$$\epsilon L_{\rm IC}(\epsilon) = u_{\rm ph}\, c\, \epsilon \int_{E_e^{\rm min}}^{E_e^{\rm max}} N_e(E_e) \frac{d\sigma(x_{\rm IC},\epsilon_0,E_e)}{dE_e} dE_e\,, \quad (28)$$

where $d\sigma(x_{\rm IC},\epsilon_0,E_e)/dE_e$ is a parametrized differential cross section for an isotropic target photon field, valid in both Th and KN regimes (Blumenthal & Gould 1970). This magnitude depends on the adimensional parameter

$$x_{\rm IC} = \frac{\epsilon}{4\epsilon_0 \left(\frac{E_e}{m_e c^2}\right)^2 \left(1 - \frac{\epsilon}{E_e}\right)}\,, \quad (29)$$

for $m_e^2c^4/(4E_e^2) < x_{\rm IC} \leq 1$, where ϵ_0 is the energy of the target photons.

We calculated $\epsilon L_{\rm synch}(\epsilon)$ and $\epsilon L_{\rm IC}(\epsilon)$ for different values of $B_{\rm bs}$ and $R_{\rm c}$, and the results are presented in Figs. 5 and 6. As seen in these figures, the synchrotron component is more luminous than the IC one in the cases of $B_{\rm bs} = 150$ G, reaching bolometric luminosities of $L_{\rm synch} \sim 10^{33}$ and 2×10^{35} erg s^{-1} for $R_{\rm c} = 10^{10}$ and 10^{11} cm, respectively. In contrast, for $B_{\rm bs} = 1$ G, the dominant radiative process is IC scattering, which leads to bolometric luminosities of $L_{\rm IC} \sim 2\times10^{32}$ erg s^{-1} and $\sim 10^{35}$ erg s^{-1} for $R_{\rm c} = 10^{10}$ and 10^{11} cm, respectively. The maximum energies achieved by photons can be as high as $E_{\rm ph}^{\rm max} \sim 1$ TeV. We note the spectral break in the synchrotron and IC emission for the case $B_{\rm bs} = 150$ G. This feature is produced by the advection of particles out from the bow-shock region. In addition, the impact of KN losses hardening the electron spectrum can also be seen in the spectral shape of the synchrotron and IC emission for $R_{\rm c} = 10^{11}$ cm and $B_{\rm bs} = 1$ G.

We accounted for $\gamma-\gamma$ absorption in the stellar field of the massive star. Since we did not focus on a particular binary/observer system geometry, we assumed an isotropic target photon field (and hence also neglected angular effects in the IC calculations). As seen in Figs. 5 and 6, the attenuation in flux can be of several orders of magnitude at energies of hundreds of GeV. In only some cases of specific geometries in the $\gamma-\gamma$ interaction, can the attenuation be very much reduced (see e.g. Khangulyan, Aharonian & Bosch-Ramon 2008).

In this work, we have focused on the high-energy emission. Radio emission is also produced by electrons that leave the bow shock well before they lose most of their energy. These particles may radiate in the radio band further down the jet and their treatment is beyond the context of this study. Because of this, we have not considered the effect of synchrotron self-absorption in the radio spectrum, and we do not make predictions in this energy range.

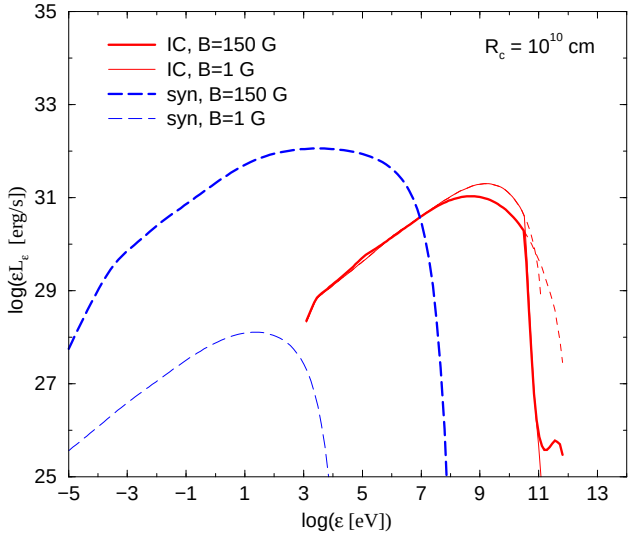

Fig. 5. Computed synchrotron (dotted line) and IC (dashed line) SEDs for the emission produced in the bow-shock region for the case of $R_{\rm c} = 10^{10}$ cm with $B_{\rm bs} = 1$ (thin line) and 150 G (thick line). The production and the $\gamma - \gamma$ absorbed curves at very high energies are shown.

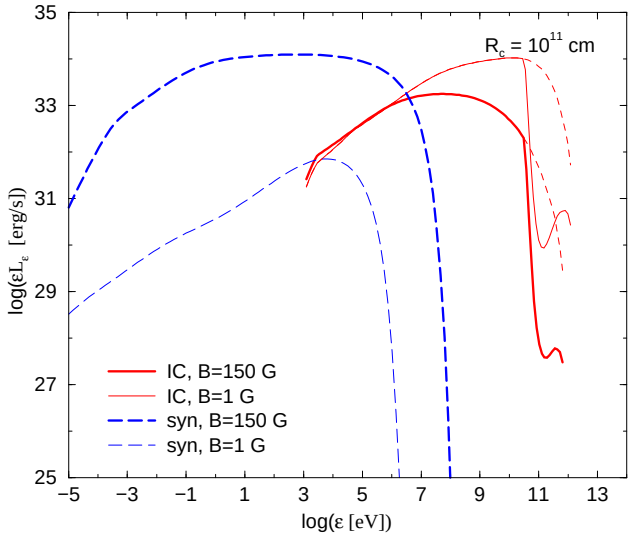

Fig. 6. The same as in Fig. 5, but for the case $R_{\rm c} = 10^{11}$ cm.

4.3. Non-thermal emission from the clump

The most energetic particles accelerated in the bow-shock region can penetrate the clump. In the case of protons, uncooled particles with $E_p > 0.025 E_p^{\rm max}$ can diffuse up to the clump and radiate only a part of their energy from there. On the other hand, for $B_{\rm bs} = 1\,{\rm G}$ ($\ll B_{\rm equipartition}$), electrons with $E_e > 0.3 E_e^{\rm max}$ will radiate their energy in the clump.

The relativistic protons that diffuse up to the clump collide with cold protons there, generating both neutral (π^0) and charged ($\pi^{\pm}$) pions that decay to γ-rays and leptons, respectively.

The emissivity of π^0 is given by

$$q_\pi(E_\pi) = c\, n_{\rm c} \int_{E_p^{\rm min}}^{E_p^{\rm max}} \sigma_{pp}(E_p) N_p(E_p) dE_p\,, \qquad (30)$$

where $\sigma_{pp}(E_p)$ is the cross section of pp interactions estimated by Kelner et al. (2006). With knowledge of the emissivity of pions, the specific luminosity of the photons produced by π^0-decay is

$$\epsilon L_\epsilon = 2\epsilon \int_{E_\pi^{\rm min}}^{E_\pi^{\rm max}} \frac{q_\pi(E_\pi)}{\sqrt{E_\pi^2 - m_\pi^2 c^4}} dE_\pi\,, \qquad (31)$$

where $E_\pi^{\rm min} = \epsilon + m_\pi^2 c^4/(4\epsilon)$ and $E_\pi^{\rm max} \sim E_p^{\rm max}/6$. The estimated emission is shown in Fig. 7, along with the contributions of the other processes. The emission reaches luminosities of as high as $L_{pp} \sim 10^{32}$ erg s^{-1} ($R_{\rm c} = 10^{11}$ cm; Fig. 7). For the adopted values of $B_{\rm bs}$ and $E_p^{\rm max}$, the $\gamma - \gamma$ absorption reduces the final fluxes and can lead to very different spectral shapes.

Secondary pairs with an effective low energy cut-off at $\sim 0.1 E_p^{\rm min}$ will be injected inside the clump by the decay of $\pi^{\pm}$. These pairs radiate most of their energy inside the clump by synchrotron, IC scattering, and relativistic bremsstrahlung. In general, primary electron emission from both the bow-shock region and the clump (see the next paragraph) is more significant than that of this secondary component (see Bosch-Ramon, Aharonian & Paredes 2005, and Orellana et al. 2007 for discussion of secondary pairs in the context of clouds and jets, respectively). Finally, we note that very high-energy neutrinos with luminosities $\sim L_{pp}$ would also be generated (e.g., Aharonian et al. 2006; Reynoso & Romero 2009).

To estimate the radiation produced by electrons accelerated in the bow-shock, we assume two values of the magnetic field of the clump: $B_{\rm c} = 1$ and 100 G, the latter being similar to the equipartition clump magnetic field.

The synchrotron and the IC radiation were calculated using the same equations given in Sect. 4.2. Regarding the relativistic bremsstrahlung, we used the standard formulae given in Blumenthal & Gould (1970). As shown in Fig. 8, synchrotron radiation is higher than IC in the case of $B_{\rm c} = 100$ G, reaching a luminosity $\sim 10^{34}$ erg s^{-1} ($R_{\rm c} = 10^{11}$ cm) at $\epsilon \sim 0.1$ MeV. For $B_{\rm c} = 1$ G, on the other hand, the absorbed IC component reaches a similar luminosity to that of the synchrotron one, $\sim 10^{33}$ erg s^{-1}. Relativistic bremsstrahlung is negligible in all cases. The SEDs for $R_{\rm c} = 10^{10}$ cm are similar to those shown in Fig. 8, but the luminosities are $\propto \sigma_{\rm c}$ and therefore two orders of magnitude less. We note that the non-thermal emission from the clump is similar to, but of slightly lower intensity than the bow shock one, being the spectra harder. We note that the radio emission produced by leptons in the clump is strongly suppressed by ionization losses and the high low-energy cut-off of the injected electrons. For clarity, we have not plotted the leptonic emission from the clump together with the other components, but they can be compared using Figs 7 and 8.

5. Discussion and summary

We explored the main physical processes and the nature of the radiation produced by the interaction between the jet of a HMMQ and a clump of the wind of the companion star. The penetration of a clump in the jet produces two shocks. One shock quickly reaches a steady state in the jet, forming a bow-like shock. The other shock propagates through the clump driven by pressure equilibrium

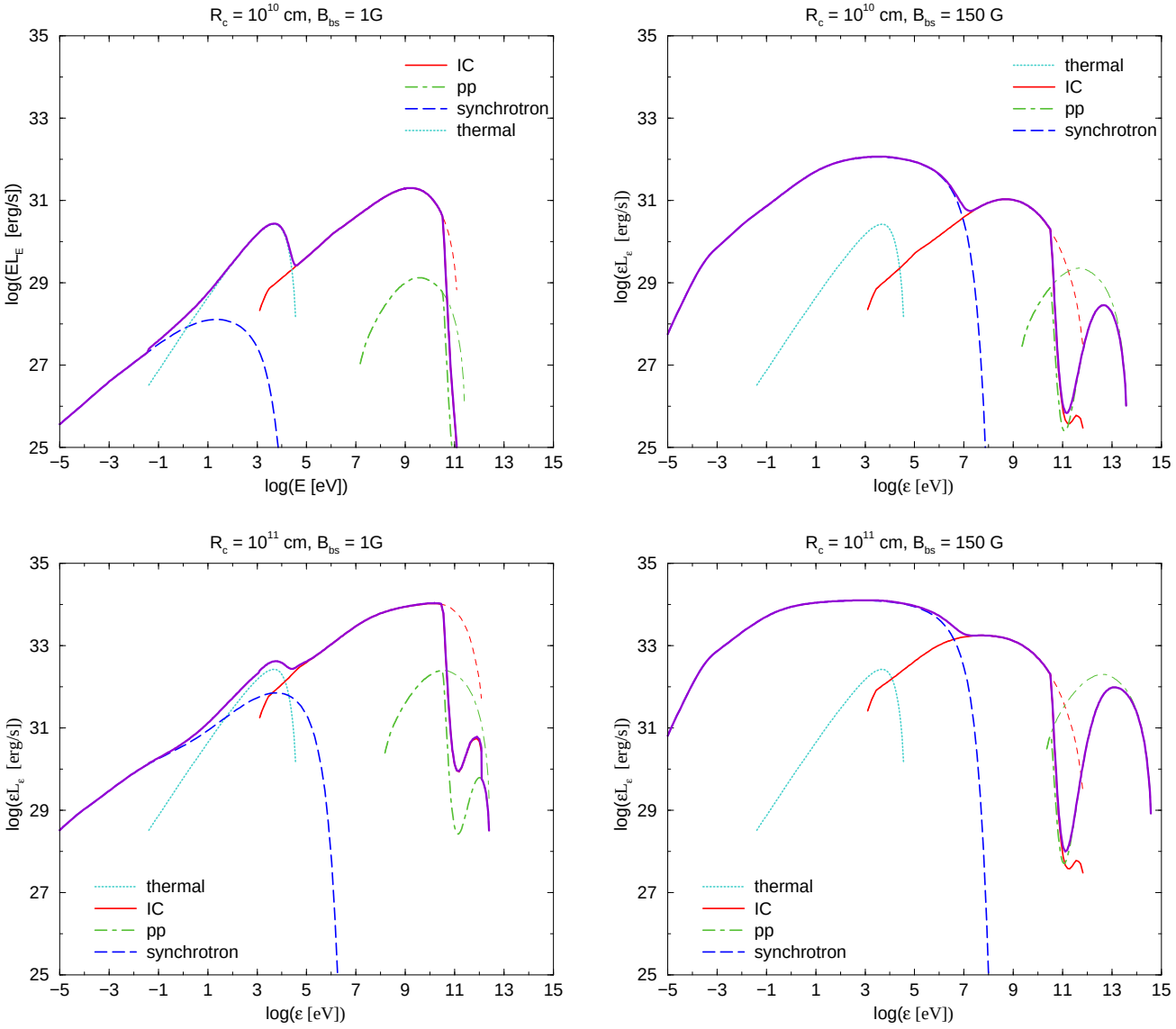

Fig. 7. SEDs for different values of $B_{\rm bs}$ and $R_{\rm c}$; the curves of both absorbed and unabsorbed (thin lines) IC and *pp* radiation are shown.

in the jet/clump contact discontinuity. The bow shock is adiabatic and fast, and particles can be accelerated to very high energies, leptons efficiently emitting synchrotron and IC radiation. Otherwise, the shock in the clump is slow and radiative. It is a non-efficient accelerator but a thermal emitter as well as a good target for proton-proton collisions. If electrons from the bow-shock region enter the clump, they could also radiate energy efficiently there via synchrotron and IC processes. The SEDs of the mentioned radiation components have been computed in the context of a microquasar with parameters similar to those of Cygnus X-1, showing that in some cases the interaction between one clump and the jet can yield significant amounts of radiation. The entire SEDs for different cases of clump size and magnetic field are shown in Figs. 7 and 8.

As noted above, given the limitations of the one-zone approximation, the synchrotron emission has been computed in the optically thin case, neglecting the impact of synchrotron self-absorption. Nevertheless, we note that the radio fluxes can be quite high, despite probably being self-absorbed right at the bow-shock region. Radio emission produced further down the jet by electrons accelerated in the bow shock may contribute significantly to the radio band, i.e., jet-clump interactions should have associated radio flares.

At X-rays, the emission is produced by synchrotron (bow shock and clump) and thermal radiation (clump). In the cases with $B_{\rm bs} \sim 1$ G, the thermal emission, reaching luminosities of $L_{\rm th} \sim 10^{32}$ erg s^{-1}, is of higher intensity than that of synchrotron from the bow-shock region, but not from the clump if $R_{\rm c} = 10^{11}$ cm. Synchrotron emission from the bow-shock region dominates in the X-rays band for $B_{\rm bs} = 150$ G and $L_{\rm synch} \sim 10^{35}$ erg s^{-1}. In a source such as Cygnus X-1, these levels of X-ray emission would be overcome by the accretion disk radiation. Nevertheless, in the case of fainter jet sources at X-rays, such as LS 5039 and LS I +61 303 (Bosch-Ramon et al. 2007, Paredes et al. 2007), the synchrotron X-rays produced during the jet-clump interaction may be detectable, and even the thermal component may be detectable on the top of a non-thermal component in certain conditions (large clumps of relatively low densities).

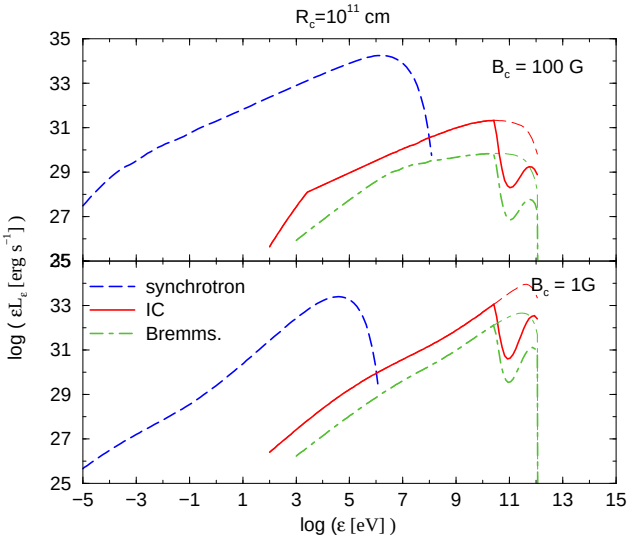

Fig. 8. Non-thermal leptonic emission from the clump, for the case $R_{\rm c} = 10^{11}$ cm and for the two assumed values of $B_{\rm c}$, 1 (bottom) and 100 G (top), is shown. The curves for both absorbed (thick lines) and unabsorbed (thin lines) IC radiation and relativistic bremsstrahlung are shown.

Inverse Compton scattering in the bow-shock region and the clump produces γ-rays up to very high energies that dominate the radiation output in cases of relatively weak magnetic fields (e.g., $B_{\rm bs} = 1$ G). In our calculations, the highest luminosity achieved is $L_{\rm IC} \sim 10^{35}$ erg s^{-1} for $R_{\rm c} = 10^{11}$ cm, although $\gamma - \gamma$ absorption can reduce the emission substantially above 100 GeV. Proton-proton collisions in the clump can also produce γ-rays at energies that may be as high as $\sim 10^{14}$ eV ($B_{\rm bs} = 150$ G). The maximum luminosity obtained by *pp* is nevertheless quite modest, $L_{pp} \sim 10^{32}$ erg s^{-1} for $R_{\rm c} = 10^{11}$ cm, although denser and/or bigger clumps, and more powerful jets may yield detectable amounts of photons outside the $\gamma - \gamma$ absorption range (0.1-10 TeV). We recall that specific geometries of the binary/observer system plus a high-energy emitter far from the compact object may render the attenuation of γ-rays much smaller (e.g., Khangulyan et al. 2008).

As a consequence of the characteristics of the interaction, the expected emission is transient. The flare duration is related to the permanence of the clump inside the jet dependent on RT and KH instabilities, which can destroy the clump. Since the clump is accelerated inside the jet, it may be disrupted after several dynamical timescales. If the clump were not destroyed, it would eventually leave the jet as a thin and moderately hot slab of plasma, since the shock in the clump is radiative. Given the typical dynamical and crossing timescales, the entire event may have a duration of between a few minutes and hours.

The flares of jet-clump interactions would have associated lower (synchrotron, thermal emission) and higher energy components (IC, *pp* emission), which should not be correlated with the accretion disk activity. The total level of emission, the importance of the different components, and the duration of the flares, can provide information about the jet power and size, clump size and density, and magnetic fields in the interaction regions (Romero et al. 2007). Therefore, besides the jet itself, the clump properties can be probed by observations at high and very high energies (and probably also at radio frequencies) of transient activity in HMMQs, which are a new tool for studying the winds of massive stars.

Depending on the wind filling factor (or clump density) and the clump size/number -$N_{\rm c}$- (Owocki & Cohen 2006), the flares produced by interactions of clumps with jets in HMMQs could be a sporadic phenomenon, for a low number of clumps, or may appear as a modulated steady activity, for a high number of clumps (see Owocki et al. 2009). For the parameters adopted here, the former case corresponds to $R_{\rm c} = 10^{11}$ cm and the latter to $R_{\rm c} = 10^{10}$ cm. Nevertheless, we note that the jet may be disrupted in those cases when too many clumps are simultaneously present inside the jet. Assuming that jet disruption takes place for $\sigma_{\rm j} < N_{\rm c} \times \sigma_{\rm c}$, for the wind and jet properties adopted in this work, the jet could be destroyed if $R_{\rm c} \lesssim 10^{10}$ cm. However, more detailed calculations of the dynamics of the jet-clump interaction are required to clarify this issue.

Acknowledgements. The authors thank Stan Owocki and Dmitry Khangulyan for many insightful discussions on clumps, jets, and hydrodynamics. A.T.A. thanks the Max Planck Institut für Kernphysik for its suport and kind hospitality. V.B-R. and G.E.R. acknowledge support by DGI of MEC under grant AYA2004-07171-C02-01, as well as partial support by the European Regional Development Fund (ERDF/FEDER). V.B-R. gratefully acknowledges support from the Alexander von Humboldt Foundation.

References

Abdo, A.A. et al. 2009 [arXiv:0902.1340]
Aharonian, F.A., & Atoyan, A.M., 1996, A&A, 309, 917
Aharonian, F.A., et al., 2005, Science, 309, 746
Aharonian, F. A., Anchordoqui, L. A., Khangulyan, D., & Montaruli, T. 2006, J.Phys.Conf.Ser., 39, 408
Albert, J., et al. 2006, Science, 312, 1771
Albert, J., et al., 2007, ApJ, 665, L51
Blumenthal, G.R., Gould, R.J., 1970, Rev. Mod. Phys., 42, 237
Bosch-Ramon, V., Aharonian, F.A., & Paredes, J.P., 2005, A&A, 432, 609
Bosch-Ramon, V., Romero, G.E., & Paredes, J.P., 2006, A&A, 447, 263
Bosch-Ramon, V., Motch, C., Ribó, M., Lopes de Oliveira, R., Janot-Pacheco, E., Negueruela, I., Paredes, J.M., & Martocchia, A., 2007, A&A, 473, 545
Bosch-Ramon, V. & Khangulyan, D., 2008, International Journal of Modern Physics D, in press (2009) [arXiv:0805.4123]
Corbel, S., Fender, R.P., Tzioumis, A.K., Tomsick, J.A., Orosz, J.A., Miller J.M., Wijnands, R., Kaaret, P., 2002, Sci, 298, 196
Drury, L.O.'C., 1983, RPPh, 46, 973
Fragile, P.C., Murray, S.D., Anninos, P. & van Breugel, W., 2004, ApJ, 604, 74
Gallo, E., Fender, R., Kaiser, C., Russell, D., Morganti, R., Oosterloo, T., & Heinz, S., 2005, Natur, 436, 819
Ginzburg, V.L., Syrovatskii, S.I., 1964, The Origin of Cosmic Rays, Pergamon Press, New York
Hillas, A.M., 1984, ARA&A, 22, 425
Kelner, S.R., Aharonian, F.A., & Vugayov, V.V., 2006, Phys. Rev. D, 74, 034018
Khangulyan, D., Aharonian, F., Bosch-Ramon, V., 2008, MNRAS, 383, 467
Klein, R.I., McKee, C.F. & Colella, P., 1994, ApJ, 420, 213
Krtička, J., & Kubát, J., 2001, A&A, 377, 175
Lang, K.R., 1999, Astrophysical Formulae, Springer, Berlin
Miller-Jones, J.C.A., Fender, R.P. & Nakar, E., 2006, MNRAS, 367, 1432
Mirabel, I.F. & Rodríguez, L.F., 1999, ARA&A 37, 409
Moffat, A.F.J., 2008, Proceedings of the conference "Clumping in hot-star winds" held in Potsdam, Germany, June 2007. Eds.: Hamann, W.R., Feldmeier, A. & Oskinova, L., 17
Orellana, M., Bordas, P., Bosch-Ramon, V., Romero, G. E., & Paredes, J. M. 2007, A&A, 476, 9
Owocki, S.P., & Cohen D.H., 2006, ApJ, 648, 5650

Owocki, S.P., Romero G.E., Townsend, R. & Araudo, A.T., 2009, ApJ (in press) [arXiv:0902.2278]
Paredes, J.M., Ribó, M., Bosch-Ramón, V., et al., 2007, ApJ, 664, L39
Paredes, J.M. 2008, Int. Jour. Mod. Phys. D, 17, 1849
Perucho, M., & Bosch-Ramon, V, 2008, A&A, 482, 917
Protheroe, R.J., 1999, in: Acceleration and Interaction of Ultra High Energy Cosmic Rays in *Topics in cosmic-ray astrophysics*, eds. M. A. DuVernois (Nova Science Publishing), p. 240 [astro-ph/9812055]
Puls, J., Markova, N., Scuderi, S., Stanghellini, C., Taranova, O.G., Burnley, A.W., Howarth I.D., 2006, A&A, 454, 625
Raga, A.C., Cantó, J., Rodríguez-González, A. & Esquivel, A., 2009, A&A, 493, 115
Reynoso, M. & Romero, G. E. 2009, A&A, 493, 1
Ribó, M., 2005, ASPC, 340, 269
Romero, G. E. & Orellana, M. 2005, A&A, 439, 237
Romero, G. E., Torres, D. F., Kaufman Bernadó, M. M., & Mirabel, I. F., 2003, A&A, 410, 1
Romero, G. E., Owocki, S. P., Araudo, A. T., Townsend, R. H. D., & Benaglia, P., in: Clumping in Hot Star Winds, W. R. Hamann, A. Feldmeier & L. M. Oskinova (eds.), Potsdam, Univ. Verl., 2008, p. 191 [atro-ph/0708.1525]
Russell, D.M., Fender, R.P., Gallo, E., & Kaiser, C.R., 2007, MNRAS, 376, 1341
van Dike & Gordon, H., 1959, NASA TR R-1
Zhekov, S.A. & Palla, F., 2007, MNRAS, 382, 1124

Astronomy & Astrophysics manuscript no. AA˙2008˙11519
June 25, 2009

High-energy emission from jet-clump interactions in microquasars

A. T. Araudo[1,2,⋆], V. Bosch-Ramon[3] and G. E. Romero[1,2,⋆⋆]

[1] Instituto Argentino de Radioastronomía (CCT La Plata, CONICET), C.C.5, 1894 Villa Elisa, Buenos Aires, Argentina
[2] Facultad de Ciencias Astronómicas y Geofísicas, Universidad Nacional de La Plata, Paseo del Bosque, 1900 La Plata, Argentina
[3] Max Planck Institut für Kernphysik, Saupfercheckweg 1, Heidelberg 69117, Germany

Received / Accepted

ABSTRACT

Context. High-mass microquasars are binary systems consisting of a massive star and an accreting compact object from which relativistic jets are launched. There is considerable observational evidence that winds of massive stars are clumpy. Individual clumps may interact with the jets in high-mass microquasars to produce outbursts of high-energy emission. Gamma-ray flares have been detected in some high-mass X-ray binaries, such as Cygnus X-1, and probably in LS 5039 and LS I+61 303.
Aims. We predict the high-energy emission produced by the interaction between a jet and a clump of the stellar wind in a high-mass microquasar.
Methods. Assuming a hydrodynamic scenario for the jet-clump interaction, we calculate the spectral energy distributions produced by the dominant non-thermal processes: relativistic bremsstrahlung, synchrotron and inverse Compton radiation, for leptons, and for hadrons, proton-proton collisions.
Results. Significant levels of emission in X-rays (synchrotron), high-energy gamma rays (inverse Compton), and very high-energy gamma rays (from the decay of neutral pions) are predicted, with luminosities in the different domains in the range $\sim 10^{32}$-10^{35} erg s^{-1}. The spectral energy distributions vary strongly depending on the specific conditions.
Conclusions. Jet-clump interactions may be detectable at high and very high energies, and provide an explanation for the fast TeV variability found in some high-mass X-ray binary systems. Our model can help to infer information about the properties of jets and clumpy winds by means of high-sensitivity gamma-ray astronomy.

Key words. Gamma-rays: theory – X-rays: binaries – Radiation mechanisms: non-thermal

1. Introduction

The mass loss in massive and hot stars is understood to occur by means of supersonic inhomogeneous winds structured as very dense and small clumps embedded in large regions of tenuous plasma. This idea is supported by considerable observational evidence of the clumpy structure of these winds (e.g. Puls et al. 2006, Owocki & Cohen 2006, Moffat 2008). However, as a consequence of the high spatial resolution necessary for a straightforward detection of the clumps, all the evidence is indirect. Hence, properties of clumps, such as size, density, and number, are not well-known.

Some massive stars are accompanied by a compact object, to which they transfer matter. This process leads to the formation of an accretion disk around the compact object and, in high-mass microquasars (HMMQs), to the generation of bipolar relativistic outflows (e.g. Mirabel & Rodríguez 1999).

Non-thermal emission has been observed in microquasar jets from radio (e.g. Ribó 2005) to X-rays (e.g. Corbel et al. 2002). At higher energies, gamma-ray radiation could also be produced in jets (e.g. Bosch-Ramon et al. 2006). A TeV flare was detected by MAGIC from the HMMQ Cygnus X-1 (Albert et al. 2007). Transient gamma-ray events may also have been detected from the high-mass X-ray binaries LS 5039 and LS I+61 303 by HESS (Aharonian et al. 2005) and MAGIC (Albert et al. 2006), respectively, as suggested by Paredes (2008). In addition, the HMMQ Cygnus X-3 might have been observed flaring in the GeV range by *AGILE* (ATels 1492, 1547 and 1585, see however Atel 1850). Both this instrument and *Fermi* also found several transient GeV sources in the Galactic plane without known counterpart (ATel 1394, Abdo et al. 2009). All this strongly variable gamma-ray emission may have a similar origin. For instance, the interaction between the jet and the stellar wind of the companion star could produce TeV flares (e.g., Romero et al. 2003, Romero & Orellana 2005, Romero et al. 2007, Albert et al. 2007, Perucho & Bosch-Ramon 2008, Owocki et al. 2009).

In this paper, we propose a model to explain these gamma-ray flares, based on the interaction between the jets of a HMMQ with wind inhomogeneities. The clumps can eventually penetrate the jet, leading to transient non-thermal activity that may release a significant fraction of the jet kinetic luminosity in the form of synchrotron, inverse Compton (IC), and proton-proton (pp) π^0-decay emission.

This work is organized as follows. In the next section, we describe the main characteristics of the scenario adopted and estimate the relevant timescales of the jet-clump inter-

Send offprint requests to: Anabella T. Araudo: *aaraudo@fcaglp.unlp.edu.ar*
⋆ Fellow of CONICET, Argentina
⋆⋆ Member of CONICET, Argentina

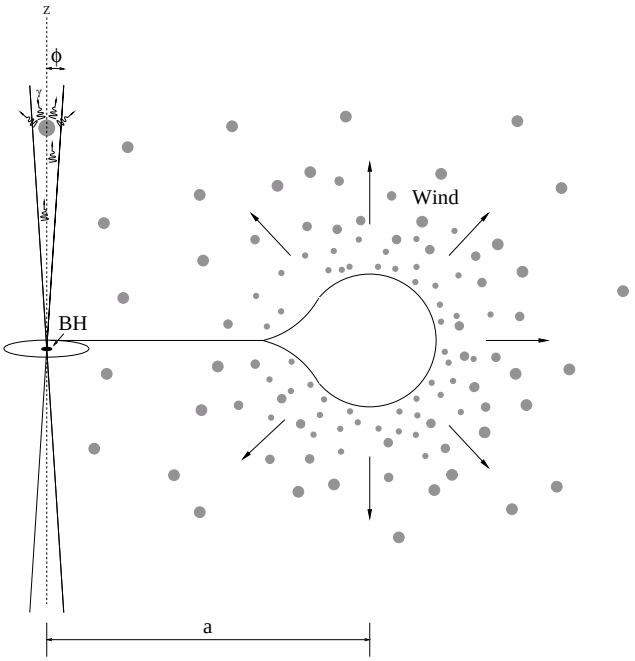

Fig. 1. Sketch of a HMMQ with clumpy stellar wind, adapted from Romero et al. (2007).

action; in Sect. 3, we study the acceleration of particles and estimate the non-thermal radiative losses; in Sect. 4, we describe the calculation of the non-thermal emission and present the main results; and finally, in Sect. 5, we draw some conclusions. CGS units are used consistently throughout the paper.

2. The physical scenario

To study the interaction between a clump of the stellar wind and a jet in a HMMQ, we adopt a scenario with similar characteristics to the binary system Cygnus X-1. We fix the separation between the compact object and the massive star to be $a = 3\times10^{12}$ cm (0.2 UA). For the star luminosity and temperature, we assume that $L_\star = 10^{39}$ erg s^{-1} and $T_\star = 3\times10^4$ K, and the stellar mass loss rate is adopted to be $\dot{M}_\star = 3\times10^{-6}\,M_\odot$ yr^{-1}, with a terminal wind velocity $v_\mathrm{w} \sim 2.5\times10^8$ cm s^{-1}. A sketch of the scenario is presented in Fig. 1.

2.1. Clump model

The clump is assumed to be spherical and homogeneous. Given the uncertainties in the clump parameters, we consider two values of its size: $R_\mathrm{c} = 10^{10}$ and 10^{11} cm (i.e., $\sim 3\times(10^{-3}-10^{-2})\,a$). For effective jet penetration, a large density contrast between the clump and the jet is required. Therefore, we assume dense clumps with $n_\mathrm{c} = 10^{12}$ cm^{-3}, which correspond to a porous clumpy wind with a filling factor (clump versus interclump volume ratio) of $f = \dot{M}_\star/4\pi a^2 m_p v_\mathrm{c} n_\mathrm{c} = 0.005$, where m_p is the mass of the proton[1]. We assume that the velocity of the clumps equals the velocity of the wind, i.e., $v_\mathrm{c} = 2.5\times10^8$ cm s^{-1}. The temperature of the clumps is taken as $T_\mathrm{c} = 10^4$ K (Krtička & Kubát 2001), which is moderately lower than the temperature at the surface of the massive star.

[1] See Owocki & Cohen (2006) for the concept of a porous wind.

Table 1. Adopted parameters in this work.

Parameter description [units]	Clump	Jet
Radius [cm]	$10^{10}-10^{11}$	1.5×10^{11}
Velocity [cm s^{-1}]	2.5×10^8	10^{10}
Density [cm^{-3}]	10^{12}	4.7×10^7
	Binary system	
System size [cm]	3×10^{12}	
Star luminosity [erg s^{-1}]	10^{39}	
Star temperature [K]	3×10^4	
Mass loss rate [M$_\odot$ yr^{-1}]	3×10^{-6}	
Wind velocity [cm s^{-1}]	2.5×10^8	

2.2. Jet model

Radio observations demonstrated that the jets of MQs are strongly collimated (Miller-Jones, Fender & Nakar 2006). We assume that the jet radius is one tenth of the jet height, i.e. $R_\mathrm{j}(z) = 0.1\,z$, which corresponds to a semi-opening angle of $\phi = 6°$. The expansion velocity results in $v_\mathrm{exp} = 0.1\ v_\mathrm{j}$, where v_j is the velocity of the jet. This expansion velocity for a free-expanding hidrodynamical jet implies a jet base Mach number $\sim v_\mathrm{j}/v_\mathrm{exp} \sim 10$, i.e. a strongly supersonic outflow. We consider a jet dynamically dominated by cold protons with a weakly relativistic bulk velocity $v_\mathrm{j} = 0.3\,c$, i.e. a Lorentz factor $\gamma_\mathrm{j} = 1.06$. We neglect the curvature of the jet produced by its interaction with the stellar wind. In HMMQ jets of luminosity $> 10^{36}$ erg s^{-1}, the geometry should not be strongly modified (Perucho & Bosch-Ramon 2008), although this effect could be important in systems such as Herbig-Haro jets interacting with a stellar wind, as studied by Raga et al. (2009).

The kinetic luminosity of the jet is taken to be $L_\mathrm{kin} \sim 3\times10^{36}$ erg s^{-1}, similar to that of Cygnus X-1 (e.g., Gallo et al. 2005, Russell et al. 2007). Using the equation

$$L_\mathrm{kin} = \sigma_\mathrm{j}(\gamma_\mathrm{j}-1)m_p\,c^2\,n_\mathrm{j}\,v_\mathrm{j}, \quad (1)$$

where $\sigma_\mathrm{j} = \pi R_\mathrm{j}^2$ is the cross-section of the jet, we can estimate the density n_j of the jet material in the laboratory reference frame (LRF). At the height of the jet-clump interaction, which is taken to occur at $z = a/2$, we obtain $n_\mathrm{j} = 4.7\times10^7$ cm^{-3}. Thus, the ratio of the clump to the jet densities is $\chi = 2.1\times10^4$. This parameter will be very relevant to the jet-clump interaction estimates. The parameter values of the clump and the jet are shown in Table 1. We assume an ideal gas equation of state, $P = nkT$, for both the clump and the jet, where n is the gas density.

2.3. Dynamics of the interaction

Clumps are formed in the wind acceleration region within one stellar radius of the surface of the star (e.g. Puls et al. 2006) and some of them reach the jet/wind interface. The very large inertia of the clumps, linked to the exceptionally high density contrast χ, allows them to cross the boundary of the jet and fully penetrate into it. A large value of χ is also required to ensure that the clump is not strongly affected when penetrating into the jet.

To study the physical processes of the interaction, we consider the collision of a single clump with the jet. For simplicity, we assume that, on the relevant spatial scales of the interaction, the jet is cylindrical. In the context of this work, thermal conduction, clump expansion, magnetic fields and gravitational forces are not dynamically relevant and will be neglected.

In the LRF, the clump will take a time $t_{\rm c}$, or jet penetration time, to fully enter the jet. This provides the first relevant timescale

$$t_{\rm c} \sim 2\,R_{\rm c}/v_{\rm c}, \tag{2}$$

which is $t_{\rm c} \sim 80$ and ~ 800 s, for $R_{\rm c} = 10^{10}$ and 10^{11} cm, respectively. In addition, the clump crosses the jet roughly at the wind velocity in the jet-crossing time

$$t_{\rm j} \sim \frac{2\,R_{\rm j}}{v_{\rm c}} = 1.2\times10^{3}\ {\rm s}. \tag{3}$$

From the moment when the clump interacts with the jet, the ram pressure exerted by the latter produces a shock in the clump, which propagates in the direction of the jet motion. Assuming that a significant fraction of the momentum flux is transferred to the clump, the clump-crossing time, which is the characteristic timescale of the jet-clump interaction, can be defined to be

$$t_{\rm cc} \sim \frac{2\,R_{\rm c}}{v_{\rm cs}} \sim \frac{2\,R_{\rm c}\sqrt{\chi}}{v_{\rm j}}, \tag{4}$$

where

$$v_{\rm cs} \sim \frac{v_{\rm j}}{\sqrt{\chi}} \tag{5}$$

is the velocity of the shock moving through the clump, derived by equating the jet/clump ram pressures. The timescale $t_{\rm cc}$ is $\sim 3\times10^{2}$ and 3×10^{3} s for $R_{\rm c} = 10^{10}$ and 10^{11} cm, respectively.

A shock (the bow shock) is also formed in the jet when its material collides with the clump. We assume that the bow-shock region width (or clump/bow-shock separation distance) is $x \sim 0.2R_{\rm c}$ (van Dyke & Gordon 1959), and thus the time required to reach the steady state regime is

$$t_{\rm bs} \sim \frac{0.2R_{\rm c}}{v_{\rm j\ ps}}, \tag{6}$$

where $v_{\rm j\ ps} \sim v_{\rm j}/4$ is the jet postshock velocity in the LRF. Therefore, $t_{\rm bs} \sim (5/2)t_{\rm cc}/\sqrt{\chi}$, i.e. $t_{\rm bs} \ll t_{\rm cc}$. In Fig. 2, a sketch of the situation is shown.

Once the clump is inside the jet, the latter transfers momentum to the clump, accelerating it to the background velocity, $v_{\rm j}$. The acceleration can be obtained from the force exerted by the jet ram pressure and the clump mass (e.g., Fragile et al. 2004):

$$g \sim \frac{v_{\rm j}^2}{\chi R_{\rm c}}\,. \tag{7}$$

The jet accelerates the clump to the velocity $v_{\rm j}$ in a time

$$t_{\rm g} \sim \frac{v_{\rm j}}{g} \sim \sqrt{\chi}\,t_{\rm cc}, \tag{8}$$

which is much longer than $t_{\rm cc}$. When one fluid exerts a force against another fluid of different density, the hydrodynamical Rayleigh-Taylor (RT) instability eventually develops,

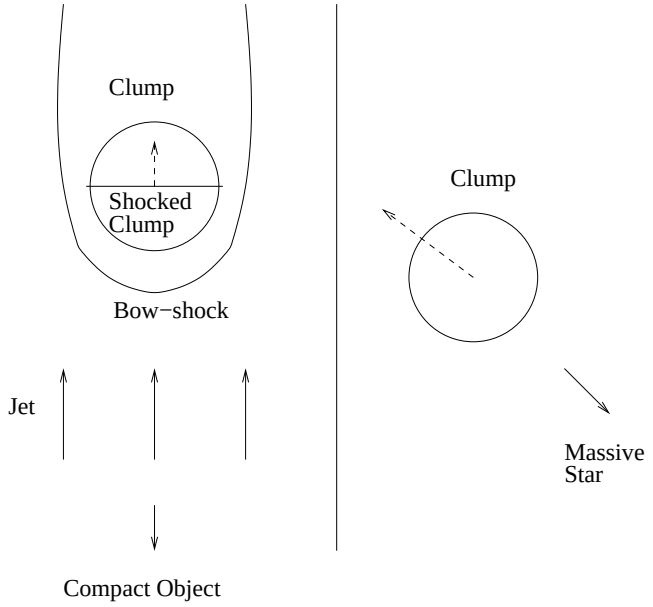

Fig. 2. Sketch of the jet-clump interaction.

leading to the perturbation and potential disruption of the clump. The timescale for this instability is

$$t_{\rm RT} \sim \sqrt{l/g}, \tag{9}$$

where l is the instability length in the perturbed region.

After the bow shock is formed, the jet material surrounds the clump and we have two fluids that have a large relative velocity. This situation leads to Kelvin-Helmholtz (KH) instabilities. The timescale for a KH instability to develop is

$$t_{\rm KH} \sim \frac{l\,\sqrt{\chi}}{v_{\rm rel}}, \tag{10}$$

where $v_{\rm rel}$ is the relative velocity between the jet material and the clump material (we assume $v_{\rm rel} \sim v_{\rm j}$). In addition, taking into account that we are interested in instability lengths similar to the clump size, i.e. $l \sim R_{\rm c}$, we find that $t_{\rm RT} \sim t_{\rm KH} \sim t_{\rm cc}$.

According to the timescales estimated in the previous paragraphs, the clump can fully enter into the jet if $t_{\rm c} \approx t_{\rm cc}/5$. At this stage, we do not consider the penetration of the clump into the jet, and assume that the former is completely inside the latter (i.e., the system has cylindrical symmetry). The bow shock is formed in a time much shorter than $t_{\rm c}$ and $t_{\rm cc}$ ($t_{\rm bs} \sim t_{\rm cc}/\sqrt{\chi}$). We note that the clump might not escape the jet if $t_{\rm j} > t_{\rm RT/KH}$. In such a case, the clump will be destroyed inside the jet. However, numerical simulations show that the instability timescales are longer than the clump crossing time by a factor of a few (e.g., Klein, McKee & Colella 1994), i.e., $t_{\rm RT/KH} > t_{\rm cc}$.

Regarding the shock properties and given the particular characteristics of our scenario, the shock in the clump is strong, radiative, and slow, whereas the bow shock is strong as well, but adiabatic and fast. For these reasons, the shocked and heated material of the clump will radiate a non-negligible part of the energy tranferred by the jet.

2.3.1. Thermal emission from the clump

To estimate the density, $n_{\rm ps}(\zeta)$, and temperature, $T_{\rm ps}(\zeta)$, of the shocked clump at a distance ζ from the shock, we assume pressure equilibrium between the clump and the jet shocked plasma and use the equation of energy flux conservation, taking into account the main channels of thermal radiative losses: $\Lambda(T) = 7\times10^{-19}\,T^{-0.6}$ erg cm^{-3} s^{-1}. The timescale of thermal cooling equals

$$t_{\rm th} = 3\times10^2\frac{T_{\rm ps}(\zeta)^{1.6}}{n_{\rm ps}(\zeta)}\,{\rm s}\,. \quad (11)$$

The temperature and density in the adiabatic zone of the post-shock region are 8.5×10^6 K and 4×10^{12} cm^{-3}, respectively. From these values, the shocked clump material cools in a time $t_{\rm th}\sim10$ s, which is shorter than $t_{\rm cc}$, which means a distance $\zeta_{\rm th}\sim t_{\rm th}\,v_{\rm cs}/4\sim2\times10^8$ cm from the shock front. Since $\zeta_{\rm th}<2R_{\rm c}$, the shock in the clump is radiative. At distances greater than $\zeta_{\rm th}$, the density of the shocked matter can reach values as high as 10^{14} cm^{-3}.

Although we are mainly interested in the high-energy emission produced by the jet-clump interaction, we estimate for comparison the free-free emission generated by the shocked and heated clump. Considering $T_{\rm ps}(\zeta)$ and $n_{\rm ps}(\zeta)$, we estimate the free-free luminosity by integrating the emissivity (Lang 1999) along the shocked clump, as demonstrated in Zhekov & Palla (2007). The corresponding thermal luminosities are $L_{\rm th}\sim5\times10^{30}$ and 5×10^{32} erg s^{-1} for $R_{\rm c}=10^{10}$ and 10^{11} cm, respectively, peaking in the soft X-rays. In Fig. 7, the thermal radiation of the clump is shown together with the non-thermal emission.

In contrast to what occurs in the clump, the bow shock is adiabatic and fast. For this reason, it is a propitious place to accelerate particles to relativistic energies.

3. Particle acceleration and non-thermal cooling

3.1. Particle acceleration

In the presence of a shock and magnetic field, non-relativistic diffusive (Fermi I) shock acceleration can occur (e.g. Drury 1983). In the linear limit of this theory and considering Bohm diffusion, electrons and protons will be accelerated to an energy $E_{e,p}$ (where e stands for electrons and p for protons) in a time

$$t_{\rm acc} = \eta\frac{E_{e,p}}{q\,B\,c}\,, \quad (12)$$

where $\eta\sim(8/3)(c/v_{\rm s})^2$ for perpendicular shocks (Protheroe 1999). In Eq. (12), $v_{\rm s}$ is the shock velocity (taken to be equal to $v_{\rm j}$), B is the magnetic field in the acceleration region, c is the speed of light, and q is the electron charge. Thus, to obtain efficient acceleration of particles, i.e., a short $t_{\rm acc}$, a high value of B and a strong and fast shock are necessary.

To study the jet-clump interaction, we consider two values of the magnetic field in the jet shocked (bow-shock) region, $B_{\rm bs}$. First, we consider a value of the magnetic field obtained by assuming that the magnetic energy density is 10 % of the plasma internal energy density downstream. We adopt a sub-equipartition value to ensure that $B_{\rm bs}$ is dynamically negligible with respect to matter. Fixing

$$\frac{B_{\rm bs}^2}{8\pi} = 0.1u_p\,, \quad (13)$$

where u_p is the energy density of the shocked jet gas, given by

$$u_p = \frac{3}{2}P = \frac{9}{8}\,n_{\rm j}\,m_p v_{\rm j}^2\,, \quad (14)$$

we obtain $B_{\rm bs}=150$ G. This magnetic field, plus $v_{\rm s}=v_{\rm j}$, yield $t_{\rm acc}\sim10^{-2}E_{e,p}$ s.

In addition, we adopt $B_{\rm bs}=1$ G to check the impact on our results of a magnetic field significantly weaker than in the sub-equipartition case.

3.2. Non-thermal cooling processes

Relativistic leptons lose their energy by different non-thermal radiative processes, such as synchrotron radiation, IC scattering and relativistic bremsstrahlung. On the other hand, relativistic protons can also lose energy by means of *pp* interactions. Finally, the shocked plasma can produce thermal radiation if the density is high enough, as shown in Sect. 2.3.1.

Relativistic electrons that lose their energy by synchrotron radiation have the following cooling time (e.g. Ginzburg & Syrovatskii, 1964)

$$t_{\rm syn} = \frac{4.1\times10^2}{B^2\,E_e}\,{\rm s}\,. \quad (15)$$

Synchrotron radiation is the most efficient radiative process in the bow-shock region in the case of $B_{\rm bs}=150$ G, where $t_{\rm synch}\sim2\times10^{-2}\,E_e^{-1}$ s.

At the interaction height considered in this work, $z_{\rm int}=a/2=1.5\times10^{12}$ cm, the energy density of the photons from the star is $u_{\rm ph}=2.4\times10^2$ erg cm^{-3}, the typical photon energy being $\epsilon_0\sim10$ eV. For $y=\epsilon_0E_e/(5.1\times10^5\,{\rm eV})^2>1$, i.e. $E_e>2.6\times10^{10}$ eV, the IC interaction occurs in the Klein-Nishina (KN) regime. A formula for the IC cooling time valid in both a Thompson (Th) and KN regime in a photon field with a narrow energy distribution is e.g. Bosch-Ramon & Khangulyan (2009)

$$t_{\rm IC} = \frac{6.1\times10^{12}\,\epsilon_0}{u_{\rm ph}}\frac{(1+8.3y)}{\ln(1+0.2\,y)}\frac{(1+1.3y^2)}{(1+0.5y+1.3y^2)}\,{\rm s}\,. \quad (16)$$

For $B\sim1$ G, IC is the dominant loss leptonic channel.

According to the low particle density of the shocked jet, $n_{\rm bs}=4\,n_{\rm j}=2\times10^8$ cm^{-3}, relativistic bremsstrahlung losses are negligible in the bow-shock region, the cooling time for a completely ionized medium being (e.g. Blumenthal & Gould, 1970):

$$t_{\rm Brem} = \frac{1.4\times10^{16}}{n\,Z^2\left(\ln\left(\frac{E_e}{m_ec^2}\right)+0.36\right)}\,{\rm s}\,, \quad (17)$$

where Z is the atomic number, and in our case $Z=1$.

Regarding hadronic emission, γ-rays are produced if relativistic protons interact with nuclei through inelastic collisions. As in the case of relativistic bremsstrahlung, the proton cooling time due to *pp* interactions depends on the density n (e.g. Aharonian & Atoyan, 1996) related

$$t_{pp}\sim\frac{2\times10^{15}}{n}\,{\rm s}\,. \quad (18)$$

In the bow-shock region, this process is negligible. Otherwise, if relativistic protons accelerated in the bow shock penetrate into the clump, *pp* interactions can become an efficient process to generate gamma-rays.

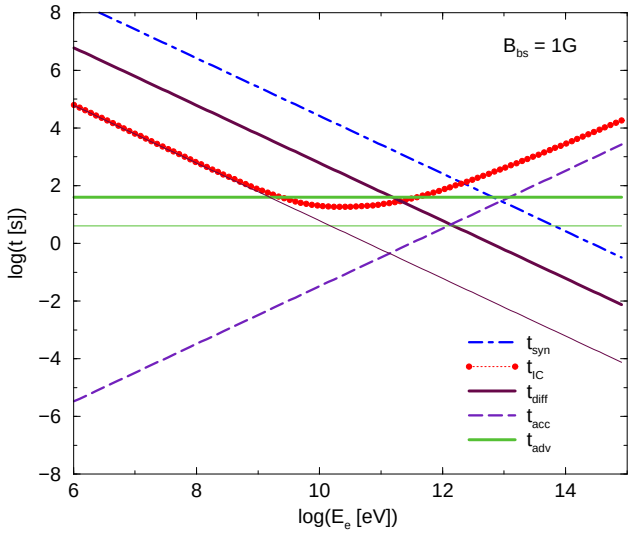

Fig. 3. Acceleration and radiative loss (synchrotron and IC) time for electrons in the bow-shock region. The advection and diffusion times are shown for $R_{\rm c} = 10^{10}$ (thin line) and 10^{11} cm (thick line). This figure corresponds to the case $B_{\rm bs} = 1$ G.

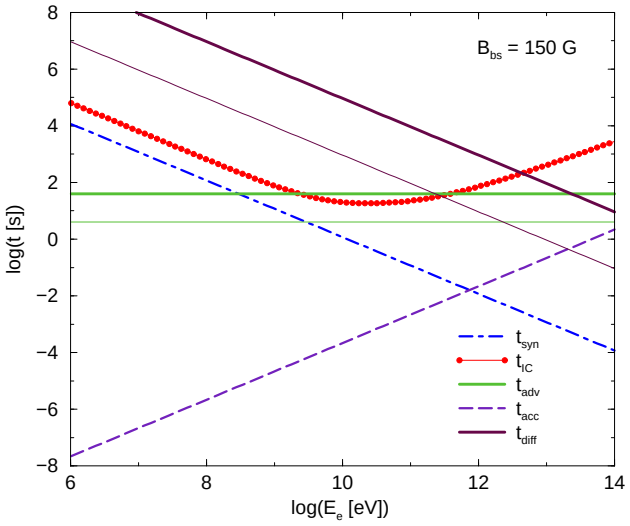

Fig. 4. Acceleration and radiative loss (synchrotron and IC) time for electrons in the bow-shock region. The advection and diffusion times are shown for $R_{\rm c} = 10^{10}$ (thin line) and 10^{11} cm (thick line). This figure corresponds to the case $B_{\rm bs} = 150$ G.

3.3. Maximum energies

Taking into account energy gains and losses, the maximum energy achieved by particles accelerated in the bow shock can be easily estimated. Concerning energy losses, we consider radiative cooling (described above) and the escape of particles. The latter takes into account the advection of relativistic particles by downstream bow-shock material ($t_{\rm adv} \sim R_{\rm c}/v_{\rm j\,ps}$) and the diffusion of particles ($t_{\rm diff} \sim x^2/2D_{\rm B}$, where $x = 0.2\,R_{\rm c}$ and $D_{\rm B} = E_{e,p}c/3qB_{\rm bs}$ is the diffusion coefficient, which is assumed to be the Böhm one). The corresponding timescale is

$$\tau_{\rm esc} = \min\{t_{\rm diff}, t_{\rm adv}\}\,. \quad (19)$$

Given the small thickness of the bow-shock region, we assume that particles that escape via diffusion go to the clump.

For electrons, the maximum energy is constrained by the escape of particles via diffusion ($B_{\rm bs} = 1$ G) and by synchrotron radiation ($B_{\rm bs} = 150$ G), as it is shown in Figs. 3 and 4. From these figures, we determine that the most relevant radiative process in the bow-shock region can be IC scattering if $B_{\rm bs} = 1$ G, and synchrotron radiation if $B_{\rm bs} = 150$ G. On the other hand, the maximum energy for protons accelerated in the bow shock is constrained by the Hillas criterion (Hillas 1984), i.e. when the proton gyroradius becomes equal to the size of the acceleration region:

$$E_p^{\rm max} = x\,q\,B_{\rm bs} = 0.2\,R_{\rm c}\,q\,B_{\rm bs}\,. \quad (20)$$

In Table 2, maximum energies for electrons and protons of different values of $B_{\rm bs}$ and $R_{\rm c}$ are shown.

4. Production of gamma-rays and lower energy radiation

We calculated the spectral energy distribution (SED) of the emission produced by the most relevant non-thermal radiative processes. In the bow-shock region, we considered synchrotron and IC radiation, and in the clump, we also considered relativistic bremsstrahlung and *pp*.

Table 2. Maximum energies achieved by acelerated particles in the bow shock. The values are in eV units and represent the different values of $R_{\rm c}$ and B studied in this work.

$R_{\rm c}$ [cm]	10^{10}	10^{10}	10^{11}	10^{11}
$B_{\rm bs}$ [G]	1	150	1	150
$E_e^{\rm max}$ [eV]	1.5×10^{11}	8×10^{11}	1.5×10^{12}	8×10^{11}
$E_p^{\rm max}$ [eV]	6×10^{11}	9×10^{13}	6×10^{12}	9×10^{14}

4.1. Distribution of relativistic particles

We assume an injected population of relativistic particles (electrons and protons) in the bow-shock region that follows a power-law energy distribution of the form

$$Q_{e,p}(E_{e,p}) = K_{e,p}\,E_{e,p}^{-\Gamma}\,\exp(-E_{e,p}/E_{e,p}^{\rm max})\,. \quad (21)$$

The index Γ is fixed to 2, typical of linear diffusive shock acceleration, and we add an exponential cut-off at high energies. The normalization constant $K_{e,p}$ is determined by assuming that 25 % of the jet luminosity incident on the bow shock, i.e. $\sim(\sigma_{\rm c}/\sigma_{\rm j})L_{\rm kin}$ (where $\sigma_{\rm c} = \pi R_{\rm c}^2$ is the clump effective cross section [2]), is converted into power of the accelerated particles. We note that the predicted fluxes scale linearly with the adopted non-thermal fraction.

To estimate the particle energy distribution $N_{e,p}$, we solve the kinetic equation in the one-zone model approximation for the bow-shock region (e.g. Ginzburg & Syrovatskii 1964)

$$\frac{\partial N_{e,p}}{\partial t} = \frac{\partial}{\partial E_{e,p}}(P_{e,p}N_{e,p}) - \frac{N_{e,p}}{\tau_{\rm esc}} + Q_{e,p}\,, \quad (22)$$

where t is the time and $P_{e,p} = -\partial E_{e,p}/\partial t$ is the energy loss rate for particles.

The relativistic leptons reach the steady state well before the shock has crossed the clump. As shown in Figs. 3

[2] We neglect here the region where the bow shock becomes strongly oblicuous, and focus on where this shock is the strongest, i.e. right in front of the clump.

and 4, the most energetic electrons can diffuse to the clump ($B_{\rm bs} = 1$ G) or lose their energy inside the bow-shock region by synchrotron and IC radiation ($B_{\rm bs} = 150$ G). However, particles downstream with low energies escape advected in the shocked material of the jet before cooling radiatively, producing a break in the energy spectrum of particles. By equating the advection and synchrotron loss times, we can estimate the break energy in the case with $B_{\rm bs} = 150$ G, which results in $E_{\rm b} = 3 \times 10^9$ and $E_{\rm b} = 3 \times 10^8$ eV, for $R_{\rm c} = 10^{10}$ and 10^{11} cm, respectively. For the case of $B_{\rm bs} = 1$ G, the break energy is determined by the advection and diffusion times, given $E_{\rm b} = 0.3 E_e^{\rm max}$. The electrons with energies $E_e > E_{\rm b}$ can reach the clump and radiate inside it. The energy distribution of these electrons is

$$N_e^{\rm c}(E_e) \sim Q_e^{\rm c}(E_e)\, t_{\rm cool}\,, \tag{23}$$

where $Q_e^{\rm c}$ is the part of Q_e that corresponds to $0.3\, E_e^{\rm max} < E_e < E_e^{\rm max}$, and $t_{\rm cool} = 1/(t_{\rm syn}^{-1} + t_{\rm IC}^{-1} + t_{\rm Brem}^{-1} + t_{\rm ion}^{-1})$. The ionization cooling term, $t_{\rm ion} \sim 2 \times 10^{18}\, (E_e/n)$ s, comes from the high densities in the clump.

As noted in Sect. 3.2, relativistic protons do not suffer significant *pp* losses in the bow-shock region ($t_{\rm diff} \ll t_{pp}$). These protons can also reach the clump if they are not advected by the shocked material of the jet. By assuming that $t_{\rm diff} < t_{\rm adv}$, the minimum energy necessary to reach the clump is

$$E_p^{\rm min} = 0.025 E_p^{\rm max}\,, \tag{24}$$

and the maximum energies of these protons are determined by the Hillas criterion and shown in Table 2. On the other hand, to confine relativistic protons in the clump, the magnetic field must be $> 10^3$ G, much stronger than the expected clump magnetic field[3], i.e., the protons will cross the entire clump in a time $\sim R_{\rm c}/c < t_{pp}$. We note that $R_{\rm c}$ should be the shocked clump width if the clump has already been affected by the shock. The distribution of relativistic protons in the clump is

$$N_p(E_p) = \frac{R_{\rm c}}{c}\, Q_p(E_p)\,. \tag{25}$$

With the steady distributions of relativistic electrons in the bow shock, $N_e(E_e)$, and of both electrons and protons in the clump, $N_e^{\rm c}(E_e)$ and $N_p(E_p)$, respectively, we can calculate the SEDs of the radiation produced by these particles.

4.2. Non-thermal emission from the bow shock

Since the energy density of the synchrotron emission is lower than that of the magnetic and stellar fields, synchrotron self-Compton processes will be neglected in our calculations.

Synchrotron radiation is computed using the standard formulae given in Blumenthal & Gould (1970). Assuming that the distribution of relativistic electrons in the bow-shock region is isotropic and moves with a non-relativistic advection speed, we calculate the synchrotron SED as

$$\epsilon L_{\rm synch}(\epsilon) = \epsilon \int_{E_e^{\rm min}}^{E_e^{\rm max}} N_e(E_e)\; P(E_e, \epsilon)\, dE_e\,, \tag{26}$$

[3] Assuming equipartition, magnetic fields ~ 100 G would be expected.

where

$$P(E_e, \epsilon) = 10^{34} B_{\rm bs} (\epsilon/E_{\rm c})^{(1/3)} \exp(-\epsilon/E_{\rm c})\, {\rm s}^{-1} \tag{27}$$

is the power function. The magnitude $E_{\rm c}(E_e) = 5.1 \times 10^{-8}\, B\, E_e^2$ erg is the characteristic energy of the produced photons.

For a thermal distribution of target photons, we can estimate the IC emission from

$$\epsilon L_{\rm IC}(\epsilon) = u_{\rm ph}\, c\, \epsilon \int_{E_e^{\rm min}}^{E_e^{\rm max}} N_e(E_e) \frac{d\sigma(x_{\rm IC}, \epsilon_0, E_e)}{dE_e} dE_e\,, \tag{28}$$

where $d\sigma(x_{\rm IC}, \epsilon_0, E_e)/dE_e$ is a parametrized differential cross section for an isotropic target photon field, valid in both Th and KN regimes (Blumenthal & Gould 1970). This magnitude depends on the adimensional parameter

$$x_{\rm IC} = \frac{\epsilon}{4\epsilon_0 \left(\frac{E_e}{m_e c^2}\right)^2 \left(1 - \frac{\epsilon}{E_e}\right)}\,, \tag{29}$$

for $m_e^2 c^4/(4E_e^2) < x_{\rm IC} \leq 1$, where ϵ_0 is the energy of the target photons.

We calculated $\epsilon L_{\rm synch}(\epsilon)$ and $\epsilon L_{\rm IC}(\epsilon)$ for different values of $B_{\rm bs}$ and $R_{\rm c}$, and the results are presented in Figs. 5 and 6. As seen in these figures, the synchrotron component is more luminous than the IC one in the cases of $B_{\rm bs} = 150$ G, reaching bolometric luminosities of $L_{\rm synch} \sim 10^{33}$ and 2×10^{35} erg s^{-1} for $R_{\rm c} = 10^{10}$ and 10^{11} cm, respectively. In contrast, for $B_{\rm bs} = 1$ G, the dominant radiative process is IC scattering, which leads to bolometric luminosities of $L_{\rm IC} \sim 2 \times 10^{32}$ erg s^{-1} and $\sim 10^{35}$ erg s^{-1} for $R_{\rm c} = 10^{10}$ and 10^{11} cm, respectively. The maximum energies achieved by photons can be as high as $E_{\rm ph}^{\rm max} \sim 1$ TeV. We note the spectral break in the synchrotron and IC emission for the case $B_{\rm bs} = 150$ G. This feature is produced by the advection of particles out from the bow-shock region. In addition, the impact of KN losses hardening the electron spectrum can also be seen in the spectral shape of the synchrotron and IC emission for $R_{\rm c} = 10^{11}$ cm and $B_{\rm bs} = 1$ G.

We accounted for $\gamma - \gamma$ absorption in the stellar field of the massive star. Since we did not focus on a particular binary/observer system geometry, we assumed an isotropic target photon field (and hence also neglected angular effects in the IC calculations). As seen in Figs. 5 and 6, the attenuation in flux can be of several orders of magnitude at energies of hundreds of GeV. In only some cases of specific geometries in the $\gamma - \gamma$ interaction, can the attenuation be very much reduced (see e.g. Khangulyan, Aharonian & Bosch-Ramon 2008).

In this work, we have focused on the high-energy emission. Radio emission is also produced by electrons that leave the bow shock well before they lose most of their energy. These particles may radiate in the radio band further down the jet and their treatment is beyond the context of this study. Because of this, we have not considered the effect of synchrotron self-absorption in the radio spectrum, and we do not make predictions in this energy range.

4.3. Non-thermal emission from the clump

The most energetic particles accelerated in the bow-shock region can penetrate the clump. In the case of protons, uncooled particles with $E_p > 0.025 E_p^{\rm max}$ can diffuse up to

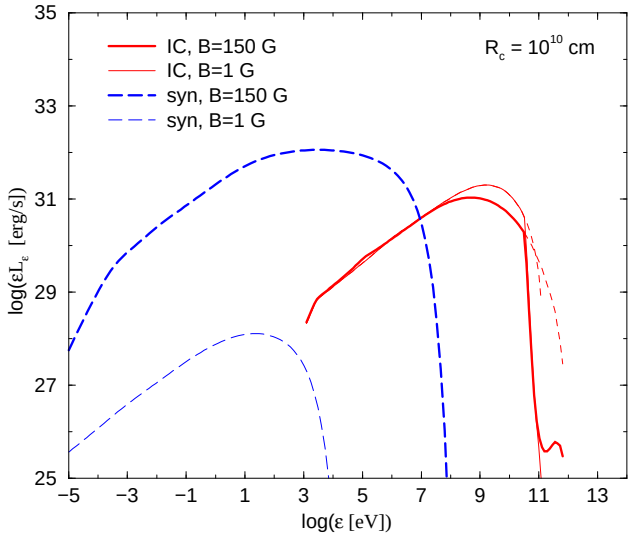

Fig. 5. Computed synchrotron (dotted line) and IC (dashed line) SEDs for the emission produced in the bow-shock region for the case of $R_{\rm c} = 10^{10}$ cm with $B_{\rm bs} = 1$ (thin line) and 150 G (thick line). The production and the $\gamma - \gamma$ absorbed curves at very high energies are shown.

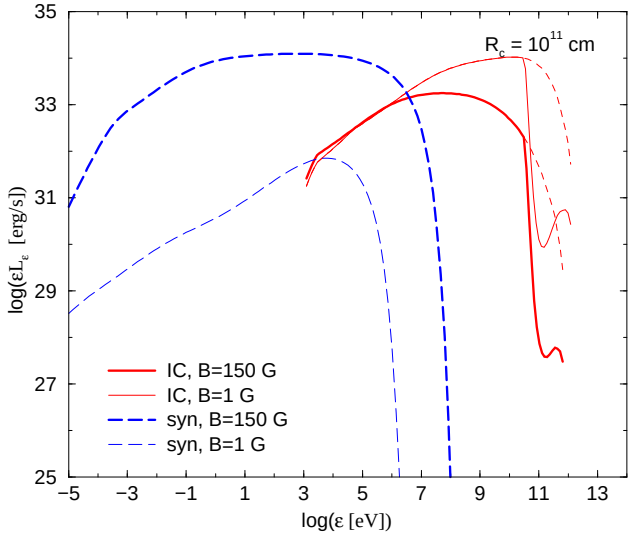

Fig. 6. The same as in Fig. 5, but for the case $R_{\rm c} = 10^{11}$ cm.

the clump and radiate only a part of their energy from there. On the other hand, for $B_{\rm bs} = 1\,{\rm G}$ ($\ll B_{\rm equipartition}$), electrons with $E_e > 0.3E_e^{\rm max}$ will radiate their energy in the clump.

The relativistic protons that diffuse up to the clump collide with cold protons there, generating both neutral (π^0) and charged ($\pi^{\pm}$) pions that decay to γ-rays and leptons, respectively.

The emissivity of π^0 is given by

$$q_\pi(E_\pi) = c\, n_{\rm c} \int_{E_p^{\rm min}}^{E_p^{\rm max}} \sigma_{pp}(E_p) N_p(E_p) dE_p\,, \qquad (30)$$

where $\sigma_{pp}(E_p)$ is the cross section of pp interactions estimated by Kelner et al. (2006). With knowledge of the emissivity of pions, the specific luminosity of the photons produced by π^0-decay is

$$\epsilon L_\epsilon = 2\epsilon \int_{E_\pi^{\rm min}}^{E_\pi^{\rm max}} \frac{q_\pi(E_\pi)}{\sqrt{E_\pi^2 - m_\pi^2 c^4}} dE_\pi\,, \qquad (31)$$

where $E_\pi^{\rm min} = \epsilon + m_\pi^2 c^4/(4\epsilon)$ and $E_\pi^{\rm max} \sim E_p^{\rm max}/6$. The estimated emission is shown in Fig. 7, along with the contributions of the other processes. The emission reaches luminosities of as high as $L_{pp} \sim 10^{32}$ erg s^{-1} ($R_{\rm c} = 10^{11}$ cm; Fig. 7). For the adopted values of $B_{\rm bs}$ and $E_p^{\rm max}$, the $\gamma - \gamma$ absorption reduces the final fluxes and can lead to very different spectral shapes.

Secondary pairs with an effective low energy cut-off at $\sim 0.1E_p^{\rm min}$ will be injected inside the clump by the decay of $\pi^{\pm}$. These pairs radiate most of their energy inside the clump by synchrotron, IC scattering, and relativistic bremsstrahlung. In general, primary electron emission from both the bow-shock region and the clump (see the next paragraph) is more significant than that of this secondary component (see Bosch-Ramon, Aharonian & Paredes 2005, and Orellana et al. 2007 for discussion of secondary pairs in the context of clouds and jets, respectively). Finally, we note that very high-energy neutrinos with luminosities $\sim L_{pp}$ would also be generated (e.g., Aharonian et al. 2006; Reynoso & Romero 2009).

To estimate the radiation produced by electrons accelerated in the bow-shock, we assume two values of the magnetic field of the clump: $B_{\rm c} = 1$ and 100 G, the latter being similar to the equipartition clump magnetic field.

The synchrotron and the IC radiation were calculated using the same equations given in Sect. 4.2. Regarding the relativistic bremsstrahlung, we used the standard formulae given in Blumenthal & Gould (1970). As shown in Fig. 8, synchrotron radiation is higher than IC in the case of $B_{\rm c} = 100$ G, reaching a luminosity $\sim 10^{34}$ erg s^{-1} ($R_{\rm c} = 10^{11}$ cm) at $\epsilon \sim 0.1$ MeV. For $B_{\rm c} = 1$ G, on the other hand, the absorbed IC component reaches a similar luminosity to that of the synchrotron one, $\sim 10^{33}$ erg s^{-1}. Relativistic bremsstrahlung is negligible in all cases. The SEDs for $R_{\rm c} = 10^{10}$ cm are similar to those shown in Fig. 8, but the luminosities are $\propto \sigma_{\rm c}$ and therefore two orders of magnitude less. We note that the non-thermal emission from the clump is similar to, but of slightly lower intensity than the bow shock one, being the spectra harder. We note that the radio emission produced by leptons in the clump is strongly suppressed by ionization losses and the high low-energy cut-off of the injected electrons. For clarity, we have not plotted the leptonic emission from the clump together with the other components, but they can be compared using Figs 7 and 8.

5. Discussion and summary

We explored the main physical processes and the nature of the radiation produced by the interaction between the jet of a HMMQ and a clump of the wind of the companion star. The penetration of a clump in the jet produces two shocks. One shock quickly reaches a steady state in the jet, forming a bow-like shock. The other shock propagates through the clump driven by pressure equilibrium in the jet/clump contact discontinuity. The bow shock is adiabatic and fast, and particles can be accelerated to very

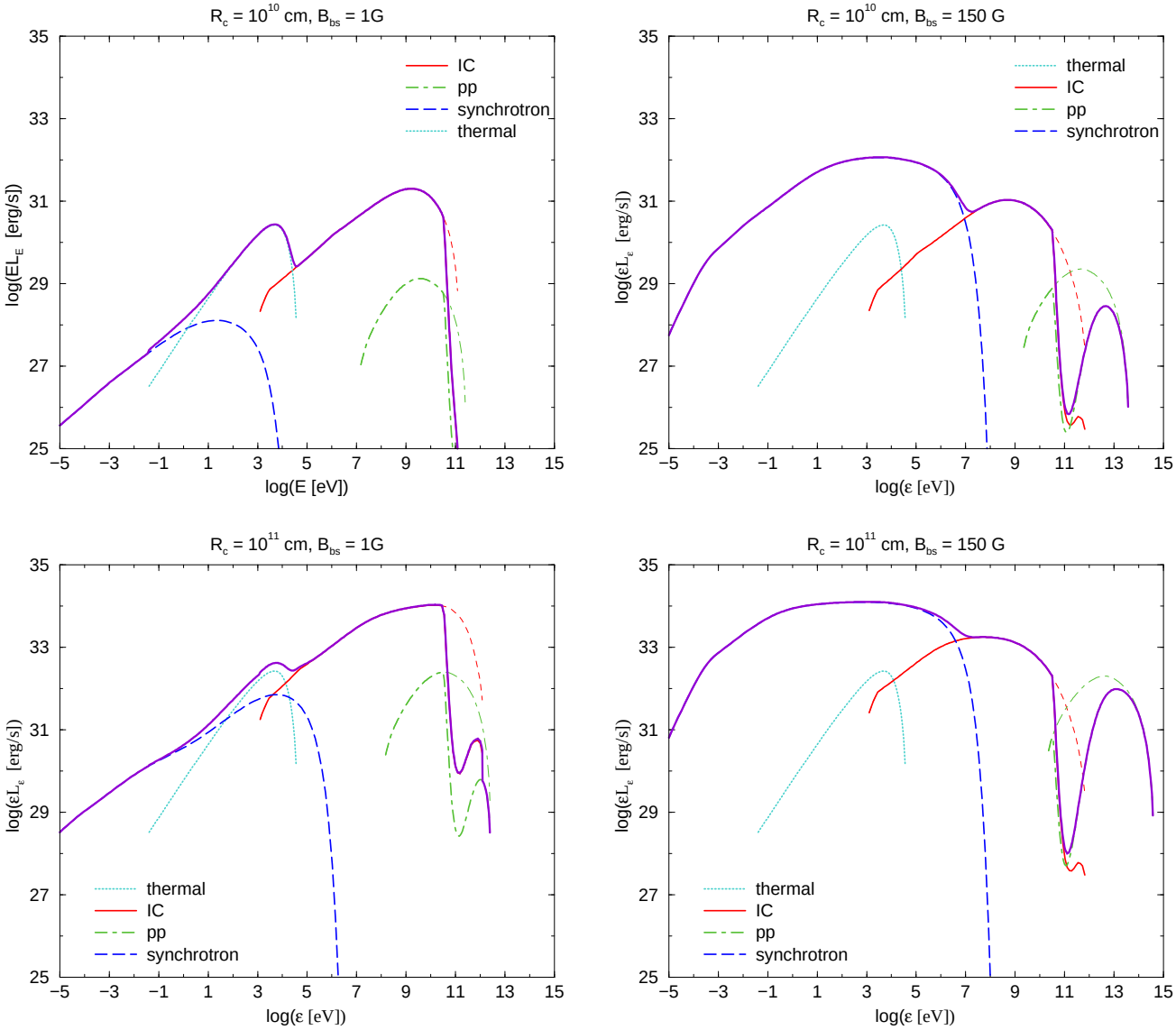

Fig. 7. SEDs for different values of $B_{\rm bs}$ and $R_{\rm c}$; the curves of both absorbed and unabsorbed (thin lines) IC and *pp* radiation are shown.

high energies, leptons efficiently emitting synchrotron and IC radiation. Otherwise, the shock in the clump is slow and radiative. It is a non-efficient accelerator but a thermal emitter as well as a good target for proton-proton collisions. If electrons from the bow-shock region enter the clump, they could also radiate energy efficiently there via synchrotron and IC processes. The SEDs of the mentioned radiation components have been computed in the context of a microquasar with parameters similar to those of Cygnus X-1, showing that in some cases the interaction between one clump and the jet can yield significant amounts of radiation. The entire SEDs for different cases of clump size and magnetic field are shown in Figs. 7 and 8.

As noted above, given the limitations of the one-zone approximation, the synchrotron emission has been computed in the optically thin case, neglecting the impact of synchrotron self-absorption. Nevertheless, we note that the radio fluxes can be quite high, despite probably being self-absorbed right at the bow-shock region. Radio emission produced further down the jet by electrons accelerated in the bow shock may contribute significantly to the radio band, i.e., jet-clump interactions should have associated radio flares.

At X-rays, the emission is produced by synchrotron (bow shock and clump) and thermal radiation (clump). In the cases with $B_{\rm bs} \sim 1$ G, the thermal emission, reaching luminosities of $L_{\rm th} \sim 10^{32}$ erg s^{-1}, is of higher intensity than that of synchrotron from the bow-shock region, but not from the clump if $R_{\rm c} = 10^{11}$ cm. Synchrotron emission from the bow-shock region dominates in the X-rays band for $B_{\rm bs} = 150$ G and $L_{\rm synch} \sim 10^{35}$ erg s^{-1}. In a source such as Cygnus X-1, these levels of X-ray emission would be overcome by the accretion disk radiation. Nevertheless, in the case of fainter jet sources at X-rays, such as LS 5039 and LS I +61 303 (Bosch-Ramon et al. 2007, Paredes et al. 2007), the synchrotron X-rays produced during the jet-clump interaction may be detectable, and even the thermal component may be detectable on the top of a non-thermal component in certain conditions (large clumps of relatively low densities).

Inverse Compton scattering in the bow-shock region and the clump produces γ-rays up to very high energies

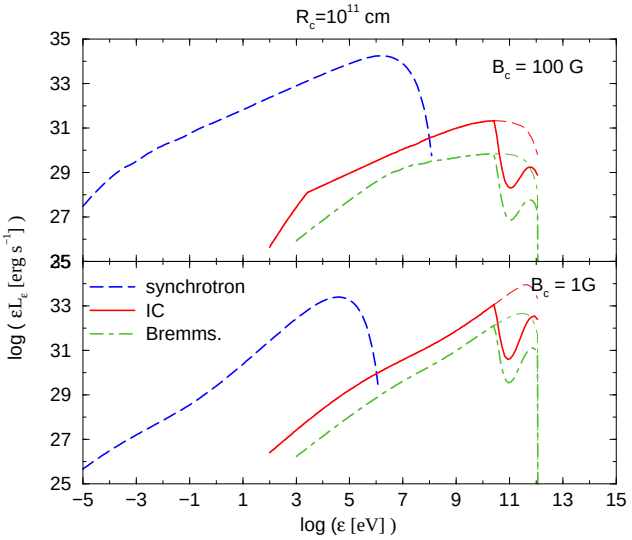

Fig. 8. Non-thermal leptonic emission from the clump, for the case $R_{\rm c} = 10^{11}$ cm and for the two assumed values of $B_{\rm c}$, 1 (bottom) and 100 G (top), is shown. The curves for both absorbed (thick lines) and unabsorbed (thin lines) IC radiation and relativistic bremsstrahlung are shown.

that dominate the radiation output in cases of relatively weak magnetic fields (e.g., $B_{\rm bs} = 1$ G). In our calculations, the highest luminosity achieved is $L_{\rm IC} \sim 10^{35}$ erg s^{-1} for $R_{\rm c} = 10^{11}$ cm, although $\gamma - \gamma$ absorption can reduce the emission substantially above 100 GeV. Proton-proton collisions in the clump can also produce γ-rays at energies that may be as high as $\sim 10^{14}$ eV ($B_{\rm bs} = 150$ G). The maximum luminosity obtained by *pp* is nevertheless quite modest, $L_{pp} \sim 10^{32}$ erg s^{-1} for $R_{\rm c} = 10^{11}$ cm, although denser and/or bigger clumps, and more powerful jets may yield detectable amounts of photons outside the $\gamma - \gamma$ absorption range (0.1-10 TeV). We recall that specific geometries of the binary/observer system plus a high-energy emitter far from the compact object may render the attenuation of γ-rays much smaller (e.g., Khangulyan et al. 2008).

As a consequence of the characteristics of the interaction, the expected emission is transient. The flare duration is related to the permanence of the clump inside the jet dependent on RT and KH instabilities, which can destroy the clump. Since the clump is accelerated inside the jet, it may be disrupted after several dynamical timescales. If the clump were not destroyed, it would eventually leave the jet as a thin and moderately hot slab of plasma, since the shock in the clump is radiative. Given the typical dynamical and crossing timescales, the entire event may have a duration of between a few minutes and hours.

The flares of jet-clump interactions would have associated lower (synchrotron, thermal emission) and higher energy components (IC, *pp* emission), which should not be correlated with the accretion disk activity. The total level of emission, the importance of the different components, and the duration of the flares, can provide information about the jet power and size, clump size and density, and magnetic fields in the interaction regions (Romero et al. 2007). Therefore, besides the jet itself, the clump properties can be probed by observations at high and very high energies (and probably also at radio frequencies) of transient activity in HMMQs, which are a new tool for studying the winds of massive stars.

Depending on the wind filling factor (or clump density) and the clump size/number -$N_{\rm c}$- (Owocki & Cohen 2006), the flares produced by interactions of clumps with jets in HMMQs could be a sporadic phenomenon, for a low number of clumps, or may appear as a modulated steady activity, for a high number of clumps (see Owocki et al. 2009). For the parameters adopted here, the former case corresponds to $R_{\rm c} = 10^{11}$ cm and the latter to $R_{\rm c} = 10^{10}$ cm. Nevertheless, we note that the jet may be disrupted in those cases when too many clumps are simultaneously present inside the jet. Assuming that jet disruption takes place for $\sigma_{\rm j} < N_{\rm c} \times \sigma_{\rm c}$, for the wind and jet properties adopted in this work, the jet could be destroyed if $R_{\rm c} \lesssim 10^{10}$ cm. However, more detailed calculations of the dynamics of the jet-clump interaction are required to clarify this issue.

Acknowledgements. The authors thank Stan Owocki and Dmitry Khangulyan for many insightful discussions on clumps, jets, and hydrodynamics. A.T.A. thanks the Max Planck Institut für Kernphysik for its suport and kind hospitality. V.B-R. and G.E.R. acknowledge support by DGI of MEC under grant AYA2004-07171-C02-01, as well as partial support by the European Regional Development Fund (ERDF/FEDER). V.B-R. gratefully acknowledges support from the Alexander von Humboldt Foundation.

References

Abdo, A.A. et al. 2009 [arXiv:0902.1340]
Aharonian, F.A., & Atoyan, A.M., 1996, A&A, 309, 917
Aharonian, F.A., et al., 2005, Science, 309, 746
Aharonian, F. A., Anchordoqui, L. A., Khangulyan, D., & Montaruli, T. 2006, J.Phys.Conf.Ser., 39, 408
Albert, J., et al. 2006, Science, 312, 1771
Albert, J., et al., 2007, ApJ, 665, L51
Blumenthal, G.R., Gould, R.J., 1970, Rev. Mod. Phys., 42, 237
Bosch-Ramon, V., Aharonian, F.A., & Paredes, J.P., 2005, A&A, 432, 609
Bosch-Ramon, V., Romero, G.E., & Paredes, J.P., 2006, A&A, 447, 263
Bosch-Ramon, V., Motch, C., Ribó, M., Lopes de Oliveira, R., Janot-Pacheco, E., Negueruela, I., Paredes, J.M., & Martocchia, A., 2007, A&A, 473, 545
Bosch-Ramon, V. & Khangulyan, D., 2008, International Journal of Modern Physics D, in press (2009) [arXiv:0805.4123]
Corbel, S., Fender, R.P., Tzioumis, A.K., Tomsick, J.A., Orosz, J.A., Miller J.M., Wijnands, R., Kaaret, P., 2002, Sci, 298, 196
Drury, L.O.'C., 1983, RPPh, 46, 973
Fragile, P.C., Murray, S.D., Anninos, P. & van Breugel, W., 2004, ApJ, 604, 74
Gallo, E., Fender, R., Kaiser, C., Russell, D., Morganti, R., Oosterloo, T., & Heinz, S., 2005, Natur, 436, 819
Ginzburg, V.L., Syrovatskii, S.I., 1964, The Origin of Cosmic Rays, Pergamon Press, New York
Hillas, A.M., 1984, ARA&A, 22, 425
Kelner, S.R., Aharonian, F.A., & Vugayov, V.V., 2006, Phys. Rev. D, 74, 034018
Khangulyan, D., Aharonian, F., Bosch-Ramon, V., 2008, MNRAS, 383, 467
Klein, R.I., McKee, C.F. & Colella, P., 1994, ApJ, 420, 213
Krtička, J., & Kubát, J., 2001, A&A, 377, 175
Lang, K.R., 1999, Astrophysical Formulae, Springer, Berlin
Miller-Jones, J.C.A., Fender, R.P. & Nakar, E., 2006, MNRAS, 367, 1432
Mirabel, I.F. & Rodríguez, L.F., 1999, ARA&A 37, 409
Moffat, A.F.J., 2008, Proceedings of the conference "Clumping in hot-star winds" held in Potsdam, Germany, June 2007. Eds.: Hamann, W.R., Feldmeier, A. & Oskinova, L., 17
Orellana, M., Bordas, P., Bosch-Ramon, V., Romero, G. E., & Paredes, J. M. 2007, A&A, 476, 9
Owocki, S.P., & Cohen D.H., 2006, ApJ, 648, 5650
Owocki, S.P., Romero G.E., Townsend, R. & Araudo, A.T., 2009, ApJ (in press) [arXiv:0902.2278]

Paredes, J.M., Ribó, M., Bosch-Ramón, V., et al., 2007, ApJ, 664, L39
Paredes, J.M. 2008, Int. Jour. Mod. Phys. D, 17, 1849
Perucho, M., & Bosch-Ramon, V, 2008, A&A, 482, 917
Protheroe, R.J., 1999, in: Acceleration and Interaction of Ultra High Energy Cosmic Rays in *Topics in cosmic-ray astrophysics*, eds. M. A. DuVernois (Nova Science Publishing), p. 240 [astro-ph/9812055]
Puls, J., Markova, N., Scuderi, S., Stanghellini, C., Taranova, O.G., Burnley, A.W., Howarth I.D., 2006, A&A, 454, 625
Raga, A.C., Cantó, J., Rodríguez-González, A. & Esquivel, A., 2009, A&A, 493, 115
Reynoso, M. & Romero, G. E. 2009, A&A, 493, 1
Ribó, M., 2005, ASPC, 340, 269
Romero, G. E. & Orellana, M. 2005, A&A, 439, 237
Romero, G. E., Torres, D. F., Kaufman Bernadó, M. M., & Mirabel, I. F., 2003, A&A, 410, 1
Romero, G. E., Owocki, S. P., Araudo, A. T., Townsend, R. H. D., & Benaglia, P., in: Clumping in Hot Star Winds, W. R. Hamann, A. Feldmeier & L. M. Oskinova (eds.), Potsdam, Univ. Verl., 2008, p. 191 [atro-ph/0708.1525]
Russell, D.M., Fender, R.P., Gallo, E., & Kaiser, C.R., 2007, MNRAS, 376, 1341
van Dike & Gordon, H., 1959, NASA TR R-1
Zhekov, S.A. & Palla, F., 2007, MNRAS, 382, 1124